TABLE 1. COMPARISON OF GENE EXPRESSION RELATED TO THE DIFFERENTIATION OF ENDODERMAL, MESODERMAL, AND ECTODERMAL LINEAGES AMONG ADIPOSE-MUSE CELLS VERSUS DERMAL- AND BM-MUSE CELLS

Mesodermal		
	Adipose / Dermal	Adipose / BM
PPARG	1.8939	3.0752
CEBPA	1.6335	0.8092
CEBPB	1.4336	1.0564
CEBPD	0.8261	0.5665
KLF15	4.2002	7.8730
LEP	0.8650	0.7210
ADIPOQ	2.3432	1.2264
AP2B1	0.7541	0.9276
FOXO1	1.9200	1.4321
SLC2A4	1.2509	1.0284
RUNX2	0.4624	0.7576
FOS	0.7956	0.3422
JUN	0.6616	0.4286
STAT1	0.7229	0.7139
SMAD1	1.0395	1.3637
SP7	Adipose only	Adipose only
ALPL	10.6316	1.5629
PAX3	0.0563	Adipose only
PAX7	Adipose only	Adipose only
MEF2C	0.4435	1.2908
TBX5	0.2465	Adipose only
KDR	2.8002	Adipose only
CXCR4	ND	BM only
NKX2-5	Dermal only	ND

Endodermal		
	Adipose / Dermal	Adipose / BM
AFP	2.0655	0.5843
ALB	ND	BM only
CD44	1.0116	1.3584
CDH1	5.3242	1.3244
CDH2	5.8358	1.4388
CTNNA1	0.9106	0.7770
CTNNB1	0.8035	0.7119
CXCR4	ND	BM only
CYP7A1	Adipose only	Adipose only
FN1	0.9322	0.8965
HNF1A	1.3105	0.9468
HNF1B	1.3378	0.4668
HNF4A	Adipose only	0.3649
HTATSF1	0.9685	1.0462
ISL1	Adipose only	0.2334
ITGA6	0.1835	0.4860
ITGB1	0.7992	0.8514
KRT7	0.7876	0.9359
NRP2	1.0134	1.0528
OTX1	0.2428	2.8003
SYP	1.0983	0.7001
THY1	0.7876	0.9118
TTR	Dermal only	ND
GATA6	4.3779	1.3704

Ectodermal		
	Adipose / Dermal	Adipose / BM
SOX2	0.2190	0.4993
NEUROG2	ND	BM only
HES1	1.8092	0.2084
HES5	0.3344	0.2169
ASCL1	Dermal only	ND
ZNF521	1.2807	13.9544
NES	0.3800	4.6525
MSI1	Adipose only	0.7347
OLIG2	ND	BM only
ISL1	Adipose only	0.2334
ISL2	0.1484	0.1060
GFAP	0.8829	Adipose only
POU3F2	1.0385	3.6332
MYT1L	Adipose only	Adipose only
NR4A2	0.5149	0.6535
DLX1	1.9342	0.2784
DLX2	6.9419	0.4366
MAP2	0.3737	0.5471
TP63	0.1497	0.0358
CRABP2	0.1967	1.2002
FN1	0.9322	0.8965
NOTCH1	0.8426	1.3712
NGFR	0.2069	0.3905
S100B	Dermal only	BM only

Expression level in adipose-Muse cells that is higher than that in dermal- or BM-Muse cells is indicated by red, whereas lower is indicated by blue colors.
BM, bone marrow.
Color images available online at www.liebertpub.com/scd

directly contribute to cell replacement or tissue regeneration [24,25]. In the true sense of functional recovery, replenishment of functional cells is essential; however, the major consensus of the primary efficacy of adipose-MSC transplantation is also attributed to trophic effects [25]. This could be explained, in part, by the small percentage of adipose-Muse cells within adipose-MSC population. However, if the ratio of adipose-Muse cells could be increased, then there may be an improvement in the curative effect of adipose-MSC transplantation. Recently, Muse cells derived from adipose tissue were reported to have been efficiently enriched from human lipoaspirated fat by long-term incubation with collagenase. Such a simple approach would be an extremely practical strategy to increase the overall yield of Muse cells for stem cell therapy [26].

BM, dermis, and adipose tissue are representative mesenchymal sources for cell-based therapy because of their easy accessibility and versatility. Even though core properties of Muse cells, namely, triploblastic differentiation, self-renewal, nontumorigenicity, and surface marker expression, are the same among those three sources, Muse cells are not the same in their gene expression that relate to endodermal-, mesodermal-, and ectodermal-lineage differentiation. Adipose-Muse cells exhibited the tendency toward expressing mesodermal lineage genes more highly than BM- and dermal-Muse cells. Conversely, genes related to endodermal and ectodermal lineages were lower in adipose-Muse cells than in those two sources. Therefore, the source for Muse cells should be selected in accordance with target tissues.

Our data show that expression of human peroxisome proliferator-activated receptor gamma (PPARγ), a gene of mesodermal lineage, in adipose-Muse cells exceeds that of dermal- and BM-Muse cells. Considering that PPARγ expression is highly sensitive to the host environment, it may play a role in the unique adipose-Muse cell response to highly stressful conditions [27]. Other mesodermal genes that are elevated in adipose-Muse cells include Krüppel-like factor 15 (KLF15) and adiponectin (ADIPOQ), which encode prominent factors in adipocyte function, further supporting the preferential adipose-Muse cell differentiation to adipocytes [26].

Genes that are downregulated in adipose-Muse cells include FOS and JUN, genes that function paradoxically in both oncogenesis and tumor suppression depending on the cell type and its differentiation state and tumor stage [28]. CDH1, which encodes Cadherin-1, was expressed more highly in adipose-Muse cells than in BM- and dermal-Muse cells. Low expression of Cadherin-1 can support tumor progression, which may allude to the absence of tumorigenesis in CDH1-rich adipose-Muse cells [29]. Further, alpha-6 integrin (ITGA6) that plays a role in mammary tumorigenesis is decreased in adipose-Muse cells as compared with dermal- and BM-Muse cells [30]. Together with low telomerase activity and nontumorigenicity, this gene expression pattern may support the safety of adipose-Muse

cells for autologous transplantation. The uniqueness in the nontumorigenicity of Muse cells has been reported previously [16,17]. Gene analysis has shown that Muse cells exhibit extremely low expression of Lin28 [17], a gene that plays a pivotal role in both maintaining pluripotency and tumorigenesis that prevail in ES and iPS cells [31]. While Muse cells retain their pluripotent capacity in the absence of a Lin28 influence [17], they reap the benefits in their insusceptibility to tumor formation. Lin28 is likely only one of the many genes that simultaneously play a role in pluripotency as well as tumorigenesis, as these two prominent aspects of stem cell character have been repeatedly described to go hand-in-hand [26,31].

It is of significance to note that ectodermal genes are primarily downregulated in adipose-Muse cells as compared with dermal- and BM-Muse cells. Important genes in neural stem cell differentiation, including HES5 and achaete-scute homolog 1 (ASCL1), are poorly expressed in adipose-Muse cells. This may indicate, perhaps, a decrease in susceptibility to neural differentiation as compared with dermal- and BM-Muse cells. Interestingly, POU domain, class 3, transcription factor 2 (POU3F2), a gene that is imperative to differentiation of pluripotent stem cells into neural cells [32], is increased in adipose-Muse cells, which suggests a capacity of adipose-Muse cells to, if not a susceptibility to, neuronal differentiation.

There exists a cohort of genes that are present only in adipose-Muse cells, and not in dermal- and BM-Muse cells. Along the mesodermal lineage, adipose-Muse cells express SP7, which encodes transcription factor Sp7, and PAX7, which encodes paired box protein Pax7. SP7 regulates osteogenic differentiation [33] and the presence of SP7 in adipose-Muse cells but not in dermal- and BM-Muse cells suggests the high capacity of adipose-Muse cells to form bone cells. It has been shown that PAX7 plays a critical role in stem cell commitment to the myosatellite cell fate, which represents a niche for a population of quiescent stem cells that have the capacity for the regeneration of muscle tissue [34,35]. PAX7 could therefore be a critical factor in the maintenance of adipose-Muse cells to remain in quiescence [26]. Along the endodermal lineage, adipose-Muse cells express CYP7A1, which encodes cholesterol 7 alpha-hydroxylase and plays a major role in maintaining hepatocyte function [36]. This supports adipose-Muse cell aptitude for differentiation into functional hepatocytes. Along the ectodermal lineage, adipose-Muse cells express MYT1L, which encodes myelin transcription factor 1-like, and thus also support the possibly of differentiation into myelin-forming cells, such as oligodendrocytes [37].

Recently, a rare population of Lin−/CD75+/CD90− pluripotent stem cells was isolated from normal human breast tissue. Similar to adipose-Muse cells, this cell population has low telomerase activity [38]. While Lin−/CD75+/CD90− cells have low tumorigenicity, adipose-Muse cells have nontumorigenic activity. This difference may be attributable in part to the expression of CD90 in adipose-Muse cells. CD90, also known as THY1, is a classical marker for mesenchymal stem cells. The role of CD90 in promoting or suppressing tumorigenesis is still controversial likely depending on the tissue target analyzed [39,40].

Several reports have indicated the presence of a population of very small cells termed very small embryonic-like stem cells (VSELs) in BM or in circulation, which like Muse cells have been described to have pluripotent potential [41]. However, other labs have failed to replicate this data, with only one lab demonstrating that VSELs could differentiate to lung epithelium [42,43]. While Muse cells do not share morphologic or molecular markers with VSELs, the current controversy in VSELs regarding the reproducibility emphasizes the importance of having both simple and reproducible protocols as an essential aspects for the utilization of cells.

Since AT-MSCs exhibited a higher concentration of Muse cells and higher propensity for cluster formation than in LA-MSCs, Muse cells can be obtained from adipose tissue rather than commercially available adipose-MSCs. Based on our results, $\sim 15\,cm^3$ human adipose tissue (eg, $4 \times 9.5\,cm^2$ subcutaneous adipose tissue) yields $\sim 3 \times 10^7$ MSCs by week 3, which contain nearly $\sim 3 \times 10^6$ of adipose-Muse cells (corresponding to nearly 9% of total adipose-MSCs; see Supplementary Fig. S1 and Table 1). Granted that one million Muse cells are required for one-time treatment, the same volume of $\sim 15\,cm^3$ adipose tissue for 1 week culturing is estimated to be necessary. Interestingly, from 1 to 2 mL of BM, $\sim 3 \times 10^7$ MSCs can be obtained after 3 weeks that contain $\sim 0.3 \times 10^6$ BM-Muse cells ($\sim$1% of BM-MSCs). From these calculations, adipose-Muse cells can be considered a realistic cell source for regenerative medicine as with BM-Muse cells. Cell safety is the most important issue for the treatment of human disorders. Adipose-Muse cells do not require additional gene transfer or artificial modifications. They are naturally preexisting stem cells in adult human adipose tissue that account for a small percentage of adipose-MSCs, which have already been applied in clinical studies. Both the capacity for differentiation and lack of teratoma formation make adipose-Muse cells an attractive source for use in the clinical setting. However, there are still several hurdles that must be overcome on the way to making these cells a viable clinical resource, beyond what is already observed in adipose stem cells utilized in the clinical setting. Therefore, future experiments must include rigorous in vivo studies that explore the functional capability and nontumorigenicity of transplanted adipose-Muse cells, as well as further evidence of consistent and predictable controlled differentiation for various directed lineages.

Acknowledgment

This study was supported by the grant aid of New Energy and Industrial Technology Development Organization (NEDO).

Author Disclosure Statement

All authors state that they have no competing financial interests.

References

1. Zuk PA, M Zhu, P Ashjian, DA De Ugarte, JI Huang, et al. (2002). Human adipose tissue is a source of multipotent stem cells. Mol Biol Cell 13:4279–4295.
2. Cho YB, WY Lee, KJ Park, M Kim, HW Yoo, et al. (2013). Autologous adipose tissue-derived stem cells for the treat-

ment of Crohn's fistula: a phase I clinical study. Cell Transplant 22:279–285.
3. Tzouvelekis A, V Paspaliaris, G Koliakos, P Ntolios, E Bouros, et al. (2013). A prospective, non-randomized, no placebo-controlled, phase Ib clinical trial to study the safety of the adipose derived stromal cells-stromal vascular fraction in idiopathic pulmonary fibrosis. J Transl Med 11:171.
4. Gimble JM, AJ Katz and BA Bunnell. (2007). Adipose-derived stem cells for regenerative medicine. Circ Res 100:1249–1260.
5. Ikegame Y, K Yamashita, S Hayashi, H Mizuno, M Tawada, et al. (2011). Comparison of mesenchymal stem cells from adipose tissue and bone marrow for ischemic stroke therapy. Cytotherapy 13:675–685.
6. Boulland JL, M Mastrangelopoulou, AC Boquest, R Jakobsen, A Noer, et al. (2013). Epigenetic regulation of nestin expression during neurogenic differentiation of adipose tissue stem cells. Stem Cells Dev 22:1042–1052.
7. Kingham PJ, DF Kalbermatten, D Mahay, SJ Armstrong, M Wiberg, et al. (2007). Adipose-derived stem cells differentiate into a Schwann cell phenotype and promote neurite outgrowth *in vitro*. Exp Neurol 207:267–274.
8. Chandra V, G Swetha, S Muthyala, AK Jaiswal, JR Bellare, et al. (2011). Islet-like cell aggregates generated from human adipose tissue derived stem cells ameliorate experimental diabetes in mice. PLoS One 6: e20615.
9. Banas A, T Teratani, Y Yamamoto, M Tokuhara, F Takeshita, et al. (2007). Adipose tissue-derived mesenchymal stem cells as a source of human hepatocytes. Hepatology 46:219–228.
10. Ruiz JC, JW Ludlow, S Sherwood, G Yu, X Wu, et al. (2010). Differentiated human adipose-derived stem cells exhibit hepatogenic capability *in vitro* and *in vivo*. J Cell Physiol 225:429–436.
11. Aurich H, M Sgodda, P Kaltwasser, M Vetter, A Weise, et al. (2009). Hepatocyte differentiation of mesenchymal stem cells from human adipose tissue *in vitro* promotes hepatic integration *in vivo*. Gut 58:570–581.
12. Okura H, A Saga, Y Fumimoto, M Soeda, M Moriyama, et al. (2011). Transplantation of human adipose tissue-derived multilineage progenitor cells reduces serum cholesterol in hyperlipidemic Watanabe rabbits. Tissue Eng Part C Methods 17:145–154.
13. Chen J, YX Tang, YM Liu, XQ Hu, N Liu, et al. (2012). Transplantation of adipose-derived stem cells is associated with neural differentiation and functional improvement in a rat model of intracerebral hemorrhage. CNS Neurosci Ther 18:847–854.
14. Lee TH and JG Yoon. (2008). Intracerebral transplantation of human adipose tissue stromal cells after middle cerebral artery occlusion in rats. J Clin Neurosci 15:907–912.
15. Valina C, K Pinkernell, YH Song, X Bai, S Sadat, et al. (2007). Intracoronary administration of autologous adipose tissue-derived stem cells improves left ventricular function, perfusion, and remodelling after acute myocardial infarction. Eur Heart J 28:2667–2677.
16. Kuroda Y, M Kitada, S Wakao, K Nishikawa, Y Tanimura, et al. (2010). Unique multipotent cells in adult human mesenchymal cell populations. Proc Natl Acad Sci USA 107:8639–8643.
17. Wakao S, M Kitada, Y Kuroda, T Shigemoto, D Matsuse, et al. (2011). Multilineage-differentiating stress-enduring (Muse) cells are a primary source of induced pluripotent stem cells in human fibroblasts. Proc Natl Acad Sci USA 108:9875–9880.
18. Pittenger MF, AM Mackay, SC Beck, RK Jaiswal, R Douglas, et al. (1999). Multilineage potential of adult human mesenchymal stem cells. Science 284:143–147.
19. Dezawa M, H Kanno, M Hoshino, H Cho, N Matsumoto, et al. (2004). Specific induction of neuronal cells from bone marrow stromal cells and application for autologous transplantation. J Clin Invest 113:1701–1710.
20. Estes BT, BO Diekman, JM Gimble and F Guilak. (2010). Isolation of adipose-derived stem cells and their induction to a chondrogenic phenotype. Nat Protoc 5:1294–1311.
21. Kuroda Y, S Wakao, M Kitada, T Murakami, M Nojima, et al. (2013). Isolation, culture and evaluation of multilineage-differentiating stress-enduring (Muse) cells. Nat Protoc 8:1391–1415.
22. Livak KJ and TD Schmittgen. (2001). Analysis of relative gene expression data using real-time quantitative PCR and the 2(-Delta Delta C(T)) Method. Methods 25:402–408.
23. Gimble J and F Guilak. (2003). Adipose-derived adult stem cells: isolation, characterization, and differentiation potential. Cytotherapy 5:362–369.
24. Venkataramana NK, SK Kumar, S Balaraju, RC Radhakrishnan, A Bansal, et al. (2010). Open-labeled study of unilateral autologous bone-marrow-derived mesenchymal stem cell transplantation in Parkinson's disease. Transl Res 155:62–70.
25. Ren G, X Chen, F Dong, W Li, X Ren, et al. (2012). Concise review: mesenchymal stem cells and translational medicine: emerging issues. Stem Cells Transl Med 1: 51–58.
26. Heneidi S, AA Simerman, E Keller, P Singh, X Li, et al. (2013). Awakened by cellular stress: isolation and characterization of a novel population of pluripotent stem cells derived from human adipose tissue. PLoS One 8: e64752.
27. Greene ME, J Pitts, MA McCarville, XS Wang, JA Newport, et al. (2000). PPARgamma: observations in the hematopoietic system. Prostaglandins Other Lipid Mediat 62:45–73.
28. Eferl R and EF Wagner. (2003). AP-1: a double-edged sword in tumorigenesis. Nat Rev Cancer 3:859–868.
29. Ceteci F, S Ceteci, C Karreman, BW Kramer, E Asan, et al. (2007). Disruption of tumor cell adhesion promotes angiogenic switch and progression to micrometastasis in RAF-driven murine lung cancer. Cancer Cell 12:145–159.
30. Ali HR, SJ Dawson, FM Blows, E Provenzano, PD Pharoah, et al. (2011). Cancer stem cell markers in breast cancer: pathological, clinical and prognostic significance. Breast Cancer Res 13: R118.
31. Thornton JE and RI Gregory. (2012). How does Lin28 let-7 control development and disease? Trends Cell Biol 22: 474–482.
32. Pang ZP, N Yang, T Vierbuchen, A Ostermeier, DR Fuentes, et al. (2011). Induction of human neuronal cells by defined transcription factors. Nature 476:220–223.
33. Nakashima K, X Zhou, G Kunkel, Z Zhang, JM Deng, et al. (2002). The novel zinc finger-containing transcription factor osterix is required for osteoblast differentiation and bone formation. Cell 108:17–29.
34. Kadi F, P Schjerling, LL Andersen, N Charifi, JL Madsen, et al. (2004). The effects of heavy resistance training and detraining on satellite cells in human skeletal muscles. J Physiol 558:1005–1012.

35. Relaix F, D Rocancourt, A Mansouri and M Buckingham. (2005). A Pax3/Pax7-dependent population of skeletal muscle progenitor cells. Nature 435:948–953.
36. Cohen JC, JJ Cali, DF Jelinek, M Mehrabian, RS Sparkes, et al. (1992). Cloning of the human cholesterol 7 alpha-hydroxylase gene (CYP7) and localization to chromosome 8q11-q12. Genomics 14:153–161.
37. Ambasudhan R, M Talantova, R Coleman, X Yuan, S Zhu, et al. (2011). Direct reprogramming of adult human fibroblasts to functional neurons under defined conditions. Cell Stem Cell 9:113–118.
38. Roy S, P Gascard, N Dumont, J Zhao, D Pan, et al. (2013). Rare somatic cells from human breast tissue exhibit extensive lineage plasticity. Proc Natl Acad Sci USA 110: 4598–4603.
39. Abeysinghe HR, Q Cao, J Xu, S Pollock, Y Veyberman, et al. (2003). THY1 expression is associated with tumor suppression of human ovarian cancer. Cancer Genet Cytogenet 143:125–132.
40. He J, Y Liu, T Zhu, J Zhu, F Dimeco, et al. (2012). CD90 is identified as a candidate marker for cancer stem cells in primary high-grade gliomas using tissue microarrays. Mol Cell Proteomics 11: M111 010744.
41. Drukala J, E Paczkowska, M Kucia, E Mlynska, A Krajewski, et al. (2012). Stem cells, including a population of very small embryonic-like stem cells, are mobilized into peripheral blood in patients after skin burn injury. Stem Cell Rev 8:184–194.
42. Kassmer SH, H Jin, PX Zhang, EM Bruscia, K Heydari, et al. (2013). Very small embryonic-like stem cells from the murine bone marrow differentiate into epithelial cells of the lung. Stem Cells. [Epub ahead of print]; DOI: 10.1002/stem.1413.
43. Miyanishi M, Y Mori, J Seita, JY Chen, S Karten, et al. (2013). Do pluripotent stem cells exist in adult mice as very small embryonic stem cells? Stem Cell Rep 1:198–208.

Address correspondence to:
Prof. Mari Dezawa
Department of Stem Cell Biology and Histology
Tohoku University Graduate School of Medicine
2-1 Seiryo-machi, Aoba-ku
Sendai 980-8575
Japan

E-mail: mdezawa@med.tohoku.ac.jp

Received for publication September 28, 2013
Accepted after revision November 18, 2013
Prepublished on Liebert Instant Online November 20, 2013

Damnacanthal, an effective inhibitor of LIM-kinase, inhibits cell migration and invasion

Kazumasa Ohashi[a], Kaori Sampei[a], Mami Nakagawa[a], Naoto Uchiumi[a], Tatsuya Amanuma[a], Setsuya Aiba[b], Masato Oikawa[c], and Kensaku Mizuno[a]

[a]Department of Biomolecular Sciences, Graduate School of Life Sciences, Tohoku University, Sendai, Miyagi 980-8578, Japan; [b]Department of Dermatology, Tohoku University Graduate School of Medicine, Sendai, Miyagi 980-8574, Japan; [c]Graduate School of Nanobioscience, Yokohama City University, Seto, Kanazawa-ku, Yokohama 236-0027, Japan

ABSTRACT LIM-kinases (LIMKs) play crucial roles in various cell activities, including migration, division, and morphogenesis, by phosphorylating and inactivating cofilin. Using a bimolecular fluorescence complementation assay to detect the actin–cofilin interaction, we screened LIMK1 inhibitors and identified two effective inhibitors, damnacanthal (Dam) and MO-26 (a pyrazolopyrimidine derivative). These compounds have already been shown to inhibit Lck, a Src family tyrosine kinase. However, in vitro kinase assays revealed that Dam inhibited LIMK1 more effectively than Lck. Dam suppressed LIMK1-induced cofilin phosphorylation and deceleration of actin retrograde flow in lamellipodia in N1E-115 cells. Dam impaired CXCL12-induced chemotactic migration of Jurkat T lymphocytes and Jurkat-derived, Lck-deficient JCaM1.6 cells and also inhibited serum-induced migration and invasion of MDA-MB-231 breast carcinoma cells. These results suggest that Dam has the potential to suppress cell migration and invasion primarily through the inhibition of LIMK kinase activity. Topical application of Dam also suppressed hapten-induced migration of epidermal Langerhans cells in mouse ears. Dam provides a useful tool for investigating cellular and physiological functions of LIMKs and holds promise for the development of agents against LIMK-related diseases. The bimolecular fluorescence complementation assay system used in this study will provide a useful method to screen for inhibitors of various protein kinases.

Monitoring Editor
Laurent Blanchoin
CEA Grenoble

Received: Sep 19, 2013
Revised: Dec 26, 2013
Accepted: Jan 17, 2014

INTRODUCTION

Actin cytoskeletal dynamics and remodeling are central to a variety of cell activities, including cell migration, division, morphogenesis, and gene expression. Among numerous actin-regulatory proteins, the actin-depolymerizing factor (ADF)/cofilin family proteins bind to G- and F-actin and play an essential role in regulating actin cytoskeletal dynamics and reorganization by severing and disassembling actin filaments (Bamburg and Wiggan, 2002; Pollard and Borisy, 2003; Ono, 2007). The actin-binding, -severing, and -disassembling activities of ADF/cofilin are inhibited by the phosphorylation of its serine residue at position 3 (Ser-3) near the N-terminus. In most cells, the level or turnover rate of Ser-3 phosphorylation of ADF/cofilin dramatically changes in response to extracellular and intracellular stimuli, crucially affecting actin dynamics and cell activities; hence, the protein kinases and phosphatases responsible for ADF/cofilin phosphorylation and dephosphorylation play essential roles in regulating actin cytoskeletal dynamics and actin-related cell activities (Meberg *et al.*, 1998; Bravo-Cordero *et al.*, 2013; Mizuno, 2013).

LIM-kinases (LIMKs), consisting of LIMK1 and LIMK2 in mammals, specifically phosphorylate ADF/cofilin at Ser-3, thereby inhibiting the actin-binding, -severing, and -disassembling activities (Arber *et al.*, 1998; Yang *et al.*, 1998). LIMKs have characteristic

This article was published online ahead of print in MBoC in Press (http://www.molbiolcell.org/cgi/doi/10.1091/mbc.E13-09-0540) on January 29, 2014.

Address correspondence to: Kensaku Mizuno (kmizuno@biology.tohoku.ac.jp) or Kazumasa Ohashi (kohashi@biology.tohoku.ac.jp).

Abbreviations used: ADF, actin-depolymerizing factor; BiFC, bimolecular fluorescence complementation; CaMK, Ca^{2+}/calmodulin-dependent kinase; CFP, cyan fluorescent protein; Dam, damnacanthal; FCS, fetal calf serum; FRAP, fluorescence recovery after photobleaching; LIMK, LIM-kinase; MAPK, mitogen-activated protein kinase; MBP, myelin basic protein; PAK, p21-activated kinase; P-cofilin, Ser-3–phosphorylated cofilin; PKC, protein kinase C; ROCK, Rho-associated kinase; TNCB, 2,4,6-trinitrochlorobenzene; VC210, Venus C-terminal fragment (210–238); VN210, Venus N-terminal fragment (1–210); WT, wild type; YFP, yellow fluorescent protein.

Supplemental Material can be found at:
http://www.molbiolcell.org/content/suppl/2014/01/28/mbc.E13-09-0540v1.DC1.html

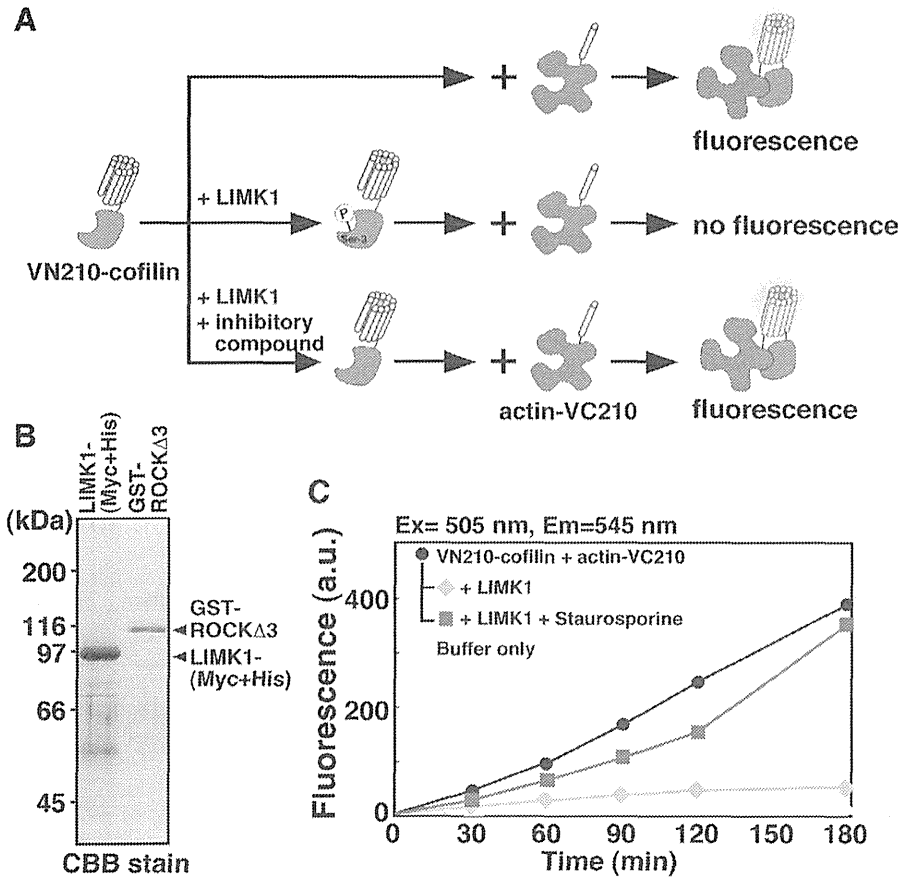

FIGURE 1: BiFC-based screening of LIMK1 inhibitors. (A) Schematic diagram of the BiFC assay used to screen for LIMK1 inhibitors. (B) Purification of LIMK1-(Myc+His) and GST-ROCKΔ3. Proteins expressed in Sf21 cells were purified, separated on SDS–PAGE, and analyzed by Coomassie brilliant blue (CBB) staining. (C) In vitro BiFC assays to detect the LIMK1-inhibiting activity of staurosporine. VN210-cofilin was preincubated with or without LIMK1, or with LIMK1 and staurosporine, and then mixed with actin-VC210. The time-dependent recovery in fluorescence of the BiFC probes is shown. a.u., arbitrary unit.

structural features, consisting of two N-terminal LIM domains, an internal PDZ-like domain, and a C-terminal protein kinase domain (Mizuno *et al.*, 1994; Okano *et al.*, 1995). The kinase domains of LIMKs contain the protein kinase consensus sequence but are unique in that they have an unusual motif (DLNSHN) in the kinase catalytic loop in subdomain VIB. Phylogenetic analysis of protein kinases places LIMKs within a tyrosine kinase-like family (Manning *et al.*, 2002). LIMKs are activated via a number of routes: phosphorylation of the conserved threonine residue in the kinase catalytic domain (Edwards *et al.*, 1999; Ohashi *et al.*, 2000; Amano *et al.*, 2001) by Rho-associated kinase (ROCK), p21-activated protein kinase (PAK), myotonic dystrophy kinase–related Cdc42-binding kinase-α (MRCKα), and Ca^{2+}/calmodulin-dependent kinase (CaMK)-II and -IV (Scott and Olson, 2007; Mizuno, 2013); phosphorylation at Ser-323 by mitogen-activated protein kinase (MAPK)–activated protein kinase-2 (MAPKAPK2); limited proteolysis at Asp-240 by caspase-3; and binding of bone morphogenic protein receptor II to the LIM domain of LIMK1 (Scott and Olson, 2007; Mizuno, 2013).

In agreement with the central role of ADF/cofilin in actin filament remodeling, previous studies demonstrated that LIMK1 plays a crucial role in diverse cell activities, including cell shape change, migration, division, and gene expression, and in pathophysiological processes, including organogenesis, cancer invasion and metastasis, angiogenesis, axon guidance, and immune and inflammatory responses (Scott and Olson, 2007; Manetti, 2012a; Mizuno, 2013). In fact, LIMK1 is activated after cell stimulation with growth factors and chemokines, and the depletion of LIMK1 suppresses cell migration and tumor cell invasion and metastasis (Nishita *et al.*, 2002, 2005; Davila *et al.*, 2003; Yoshioka *et al.*, 2003; Wang *et al.*, 2007; Horita *et al.*, 2008; Mishima *et al.*, 2010; Scott *et al.*, 2010). To explore the functional roles of LIMKs in cellular and pathophysiological processes, it is useful to identify the chemical compounds that specifically inhibit the kinase activity of LIMKs. Several inhibitors of LIMKs have been reported (Ross-Macdonald *et al.*, 2008; Harrison *et al.*, 2009; Sleebs *et al.*, 2011; Prudent *et al.*, 2012), but more potent and selective LIMK inhibitors are needed for the development of effective therapeutic agents against LIMK-related diseases such as cancer metastasis, glaucoma, and neurological and cardiovascular disorders (Manetti, 2012a,b).

We recently developed a new bimolecular fluorescence complementation (BiFC) assay system to detect the interaction between G-actin and cofilin (Ohashi *et al.*, 2012). This assay is based on the reassembly of fluorescent Venus, a variant of yellow fluorescent protein (YFP; Nagai *et al.*, 2002), from its nonfluorescent fragments. The reassembly occurs in a manner dependent on the interaction between two proteins of interest fused to each fragment (Kerppola, 2009). In the cofilin–actin interaction BiFC assay, incubation of the actin probe with the wild-type (WT) cofilin probe resulted in fluorescence; however, incubation with the phosphomimic S3E-cofilin mutant probe (with a replacement of Ser-3 by Glu) did not (Ohashi *et al.*, 2012), indicating that the recovery of Venus fluorescence reflects the nonphosphorylated state of cofilin at Ser-3. Because LIMK-mediated cofilin phosphorylation blocks the cofilin–actin interaction, the BiFC assay is an ideal tool for screening LIMK inhibitors.

In this study, LIMK1 inhibitors were screened using the in vitro BiFC assay. One compound, damnacanthal (3-hydroxy-1-methoxy-9,10-dioxoanthraquinone-2-carbaldehyde [Dam]), was identified as an effective inhibitor of LIMK1. Using Dam, we explored the role of LIMK in cell migration and invasion, confirming its use as a powerful tool for analyzing cellular and physiological functions of LIMK.

RESULTS

A BiFC-based screen of LIMK1 inhibitors

The in vitro BiFC assay system was previously developed to detect the interaction between actin and cofilin. The assay uses a pair of probes composed of the C-terminal fragment (amino acids 210–238) of Venus fused to the C-terminus of actin (actin-VC210) and the N-terminal fragment (amino acids 1–210) of Venus fused to the N-terminus of cofilin (VN210-cofilin; Figure 1A; Ohashi *et al.*, 2012).

The assay is based on the complementary reassembly of the fluorescent protein Venus from its nonfluorescent fragments (VC210 and VN210), whose association depends on the interaction between actin and cofilin (Ohashi *et al.*, 2012). Incubation of actin-VC210 with VN210-cofilin(WT) results in Venus fluorescence; however, incubation of actin-VC210 with phospho-mimic VN210-cofilin(S3E) does not recover fluorescence, indicating that phosphorylation of cofilin at Ser-3 prevents fluorescence recovery of the BiFC probes (Ohashi *et al.*, 2012). LIMK1 phosphorylates cofilin at Ser-3 and inhibits the actin–cofilin interaction; hence, incubation of VN210-cofilin with LIMK1 inhibits recovery of BiFC probe fluorescence, whereas coincubation with LIMK1 and LIMK-inhibitory compound(s) recovers fluorescence by abolishing LIMK1-mediated cofilin phosphorylation (Figure 1A). To perform the BiFC assay, we individually expressed hexahistidine (His_6)-tagged actin-VC210 and VN210-cofilin in Sf9 cells and purified them as previously reported (Ohashi *et al.*, 2012). Similarly, we individually expressed (Myc+His)-tagged LIMK1 and glutathione *S*-transferase (GST)–tagged active ROCK (ROCKΔ3) in Sf21 cells and purified them (Figure 1B). LIMK1 was preincubated with GST-ROCKΔ3 to fully activate LIMK1 (Ohashi *et al.*, 2000). The in vitro BiFC assay was performed as follows: LIMK1 was first incubated with ROCKΔ3 and ATP for 10 min, with chemical compounds for 5 min, and then with VN210-cofilin for 60 min at 30°C. The actin-VC210 probe was then added and incubated for another 30–180 min at 30°C. As previously reported (Ohashi *et al.*, 2012), when VN210-cofilin was incubated with actin-VC210 without LIMK1 preincubation, fluorescence intensity gradually increased (Figure 1C). By contrast, when VN210-cofilin was preincubated with LIMK1 and then incubated with actin-VC210, fluorescence recovery was markedly suppressed (Figure 1C). The addition of the general protein kinase inhibitor staurosporine to the preincubation mixture blocked LIMK1-mediated inhibition of fluorescence recovery and resulted in increase in fluorescence intensity (Figure 1C), demonstrating that the in vitro BiFC assay can be used to screen for LIMK1 inhibitors.

Identification of Dam and MO-26 as LIMK1 inhibitors

We used a library of 958 small–molecular weight compounds that consists of 209 known inhibitors (including anticancer drugs), three natural compounds, and 746 chemically synthesized compounds. The chemically synthesized compounds were designed to consist of unbiased compounds (Kusumoto and Oikawa, 2001; Oikawa *et al.*, 1995, 2005; Oikawa, 2010). The library was screened for LIMK1 inhibition using the in vitro BiFC assay. Four compounds (daunorubicin, doxorubicin, MO-204, and MO-273) were excluded from the screen because of their high intrinsic fluorescence. Three compounds (staurosporine, Dam, and MO-26) clearly exhibited recovery of BiFC probe fluorescence in the presence of LIMK1 (Figure 2A). Dam is a natural product purified from the roots of a tropical plant native to Thailand, *Morinda citrifolia* (*Noni* or *Yor* in Thai; Figure 2B; Faltynek *et al.*, 1995). MO-26 is a chemically synthesized pyrazolo-[3,4-*d*]pyrimidine derivative, and its structure (Figure 2B) is closely related to that of a Lck inhibitor, A-420983 (Borhani *et al.*, 2004). Dam and MO-26 were reported to inhibit Lck, a member of the Src family tyrosine kinases (Faltynek *et al.*, 1995; Burchat *et al.*, 2002). Detailed in vitro BiFC assays were conducted (Figure 2B), which demonstrated that these compounds inhibited the kinase activity of LIMK1 in the micromolar (5–10 μM) range.

Specificity of Dam and MO-26 inhibition of LIMK1 kinase activity

To determine the specificity of Dam and MO-26, we tested the compounds against the activity of various protein kinases, including LIMK1, LIMK2, Lck, and Src, using in vitro kinase assays. Protein kinases were expressed in COS-7 cells, purified by immunoprecipitation, and then subjected to in vitro kinase assays in the presence of [γ-^{32}P]ATP, substrate proteins (cofilin for LIMK1 and LIMK2; myelin basic protein [MBP] for other kinases), and various concentrations of inhibitors. Dam exhibited effective inhibition toward LIMK1, LIMK2, and Lck kinase activities, weak inhibition toward Src kinase activity (Figure 3A), and no inhibition of ROCK, PAK3, protein kinase C (PKC)-α, and CaMKIα kinase activities (Supplemental Figure S1A). The half-maximal inhibitory concentrations (IC_{50}) of Dam for LIMK1 (0.80 μM), LIMK2 (1.53 μM), and Lck (1.62 μM) were lower than those for Src, ROCK, PAK3, PKCα, and CaMKIα (>20 μM; Figure 3B and Table 1), indicating that Dam is an

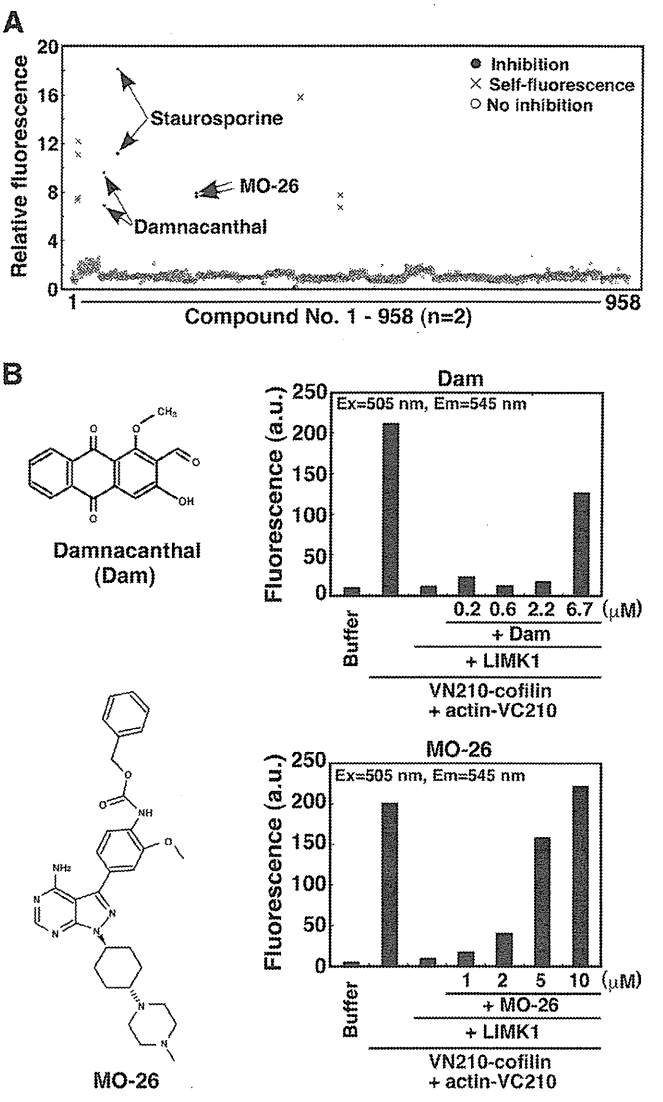

FIGURE 2: Identification of Dam and MO-26 as LIMK1 inhibitors. (A) Screening of LIMK1 inhibitors. The in vitro BiFC assay was carried out in duplicate for each chemical compound as described in *Materials and Methods*. Recovery of fluorescence intensity was calculated relative to the control. Four compounds (indicated as x) had intrinsic fluorescence. (B) LIMK1-inhibiting activity of Dam and MO-26. In vitro BiFC assays were conducted with a range of inhibitor concentrations as described in *Materials and Methods*. The chemical structures of Dam and MO-26 are shown on the left.

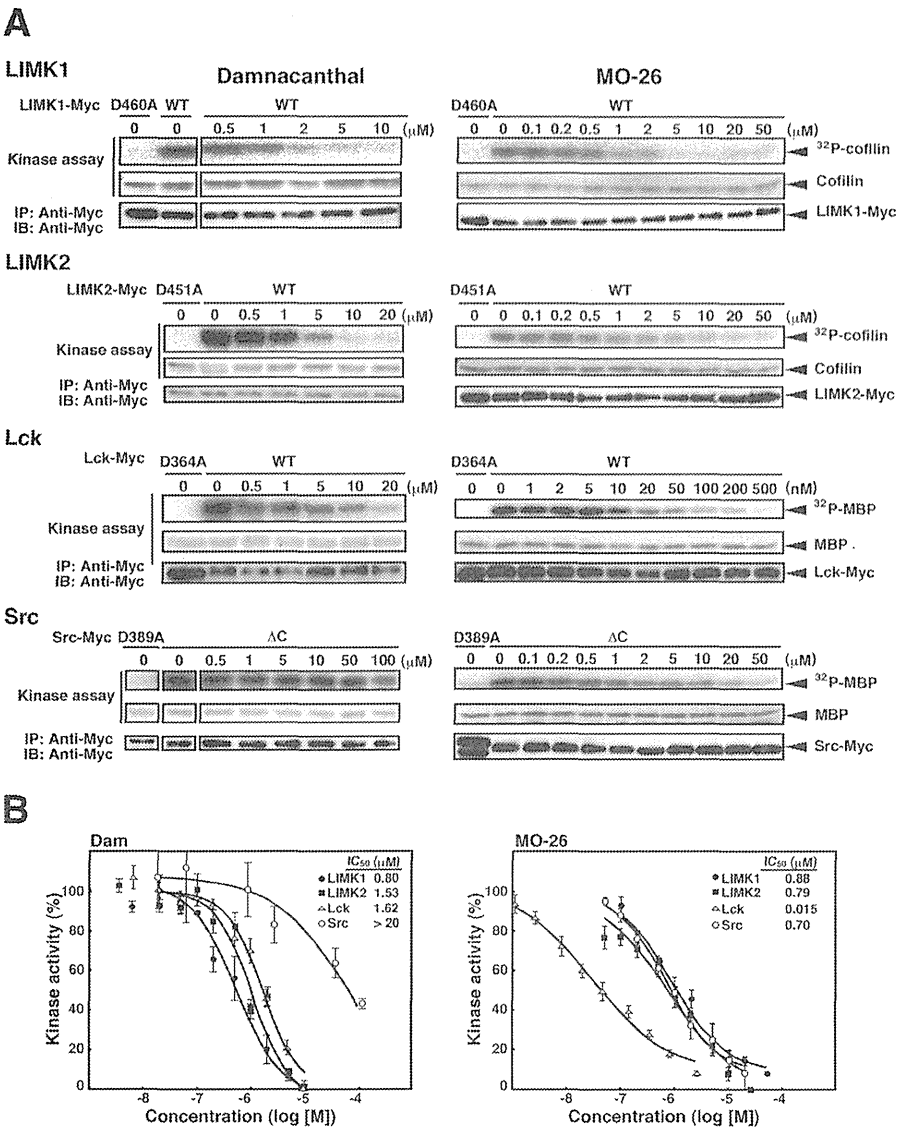

FIGURE 3: The effect of Dam and MO-26 on the kinase activity of LIMK1, LIMK2, Lck, and Src. (A) Dose-dependent effect of Dam and MO-26 on the kinase activity of LIMK1, LIMK2, Lck, and active Src (Src(ΔC)). Myc-tagged protein kinases were expressed, purified, and subjected to in vitro kinase assays, using cofilin or MBP as a substrate, in the presence of Dam or MO-26 as described in *Materials and Methods*. Kinase-inactive mutants, LIMK1(D460A), LIMK2(D451A), Lck(D364A), and Src(D389A), were used as controls. (B) Dose-dependent curves of the inhibition of kinase activity by Dam and MO-26. Data are mean values ± SD of three independent experiments.

effective inhibitor of LIMK1/2 and Lck and inhibits LIMK1 more effectively than its previously reported target, Lck. MO-26 inhibited LIMK1 and LIMK2 with an efficacy similar to that of Dam; however, it was more effective against Lck (Figure 3, A and B), with an IC_{50} value of 0.015 μM that was ~50 times lower than that for LIMK1 (0.88 μM), LIMK2 (0.79 μM), or Src (0.70 μM; Figure 3B and Table 1). MO-26 showed no inhibition of ROCK, PAK3, PKCα, and CaMKIα (IC_{50} > 20 μM; Table 1 and Supplemental Figure S1B), demonstrating that MO-26 has the potential to inhibit LIMK1, LIMK2, Src, and Lck, with particular efficacy toward Lck. Because Dam inhibited LIMK1 more effectively than Lck, the following experiments focused on the effects of Dam on the cellular functions of LIMK1.

To further examine the specificity of Dam, we analyzed the effect of Dam on the profile of phosphorylated proteins in cultured cells. We analyzed the changes in the profile of ^{32}P-labeled proteins between cell extracts from untreated and Dam-treated cells by two-dimensional (2D) gel. Autoradiography and immunoblot analysis of 2D gels showed that the amount of Ser-3–phosphorylated cofilin (P-cofilin, indicated by arrows) decreased in Dam-treated cells compared with that in untreated cells, whereas no appreciable difference in the profile of ^{32}P-labeled proteins other than P-cofilin was observed, as a whole (Supplemental Figure S2). This suggests that the pathway of cofilin phosphorylation is at least one of the major targets of Dam.

Structural requirements for the LIMK1-inhibiting activity of Dam

Dam is an anthraquinone derivative with a structure related to that of other anthraquinone derivatives, emodin and mitoxantrone (Supplemental Figure S3, A and B). Emodin inhibits Lck with an IC_{50} of 18.5 μM (Jayasuriya *et al.*, 1992), and mitoxantrone is used as an anticancer agent (Parker *et al.*, 2010); hence these compounds were examined for efficacy against LIMK1 kinase activity. However, in vitro kinase assays demonstrated that at concentrations of 1–30 μM, emodin and mitoxantrone had no appreciable effect on the kinase activity of LIMK1 (Supplemental Figure S3, A and B), indicating that the side-chain structure of Dam plays an important role in its inhibition of LIMK1.

Dam has an aldehyde group on an anthraquinone ring. To examine the function of this group, we analyzed the effect of a nucleophilic agent, hydroxylamine, on the LIMK1-inhibiting activity of Dam. Preincubation of Dam with hydroxylamine almost completely blocked the inhibitory activity of Dam (Supplemental Figure S4A). Hydroxylamine alone had no effect on LIMK1 activity. These results suggest that the aldehyde group of Dam is involved in the LIMK1-inhibiting activity of Dam.

To examine whether Dam reversibly or irreversibly inhibits LIMK1, we analyzed the effect of repeated washout on the inhibitory activity of Dam. Cyan fluorescent protein (CFP)–tagged LIMK1 was immunoprecipitated and treated with Dam or untreated for 10 min and then the precipitates were washed three times with the kinase reaction buffer or left unwashed. The LIMK1-inhibiting activity of Dam was not affected by repeated washing (Supplemental Figure S4B). Thus it is presumed that Dam may irreversibly inhibit LIMK1 by forming a stable adduct with LIMK1.

Kinase	Dam (μM)	MO-26 (μM)
LIMK1	0.80	0.88
LIMK2	1.53	0.79
Lck	1.62	0.015
Src	>20	0.70
ROCK	>20	>20
PAK3	>20	>20
PKCα	>20	>20
CaMKIα	>20	>20

IC_{50} values were determined by in vitro kinase assays using cofilin (for LIMK1 and LIMK2) and MBP (for other kinases) as substrates. See Figure 3 and Supplemental Figure S1.

TABLE 1: IC_{50} values of Dam and MO-26 toward the kinase activities of LIMKs and other protein kinases.

Dam inhibits LIMK1-mediated cofilin phosphorylation and deceleration of actin retrograde flow in cultured N1E-115 cells

Previous studies showed that overexpression of LIMK1 slows the rate of actin retrograde flow in the lamellipodia by phosphorylating and inactivating cofilin (Ohashi *et al.*, 2011). To examine whether Dam can inhibit LIMK1 activity within living cells, we analyzed the effect of Dam on LIMK1 overexpression–induced deceleration of actin retrograde flow in the lamellipodia of active RacV12-expressing N1E-115 neuroblastoma cells by fluorescence recovery after photobleaching (FRAP) time-lapse analysis of YFP-actin. After cotransfection of the cells with YFP-actin and RacV12, YFP-actin fluorescence in a rectangular region of lamellipodium was photobleached, and signal recovery was monitored every second for 40 s (Figure 4A). Kymograph analysis showed that the tip of the lamellipodium did not move substantially during time-lapse observations and that YFP-actin fluorescence was recovered gradually from the tip of the lamellipodium and moved inward at a near-constant rate via actin retrograde flow (Figure 4A, control). The rate of actin retrograde flow was measured as the rate at which the boundary between the bright and dark areas of the YFP-actin signal migrated inward from the initial cell margin. In lamellipodia of control RacV12-expressing cells, the average rate of actin retrograde flow was 5.7 μm/min (Figure 4B, control). As reported (Ohashi *et al.*, 2011), the rate of actin retrograde flow was markedly decreased in LIMK1-CFP–overexpressing cells (2.0 μm/min) compared with the rate in control cells (Figure 4, A and B). Immunoblot analysis of cell lysates showed that the amount of LIMK1-CFP was ~10 times higher than that of endogenous LIMK1 (Figure 4C). Considering the transfection efficiency of LIMK1-CFP into N1E-115 cells (~40%), the amount of LIMK1-CFP was estimated to be 25 times higher than that of endogenous LIMK1 in LIMK1-CFP–overexpressing cells. When LIMK1-overexpressing cells were pretreated with Dam at concentrations of 0.3–10 μM for 30 min and then subjected to FRAP time-lapse analysis, the decelerating effect of LIMK1 overexpression on the actin retrograde flow was significantly inhibited by Dam in the 3–10 μM range (Figure 4, A and B). To examine whether the effect of Dam on the actin retrograde flow is the result of LIMK1 inhibition, we analyzed the effect of Dam on the level of cofilin phosphorylation. The level of P-cofilin was drastically increased in LIMK1-CFP–overexpressing cells but significantly decreased in the cells after exposure to 5–10 μM Dam (Figure 4D). No apparent change in the level of total cofilin was observed. These results suggest that Dam is cell permeable and has the potential to inhibit LIMK1 kinase activity and cofilin phosphorylation in N1E-115 cells.

Dam inhibits chemotactic migration of Jurkat cells and Lck-deficient JCaM1.6 cells

It was previously reported that Dam inhibits CXCL12 (SDF-1)-induced chemotactic migration of Jurkat T-cells by inhibiting the kinase activity of Lck (Inngjerdingen *et al.*, 2002); however, LIMK1 is also required for CXCL12-induced chemotaxis in Jurkat cells (Nishita *et al.*, 2002, 2005). The results given here demonstrate that Dam inhibits the kinase activity of LIMK1 more effectively than that of Lck. Thus, to determine whether Dam suppresses the chemotactic response of Jurkat cells through Lck inhibition or through LIMK1 inhibition, we examined the effect of Dam on CXCL12-induced chemotaxis of both Jurkat and Jurkat-derived, Lck-deficient JCaM1.6 cells. Immunoblot analyses revealed that Lck was expressed in Jurkat cells but not in JCaM1.6 cells, whereas LIMK1 expression was similar in both cells (Figure 5A). Chemotactic migration was analyzed using Transwell chambers in which CXCL12 was added to the lower chamber. When Jurkat and JCaM1.6 cells were pretreated with Dam for 30 min and then subjected to chemotaxis assays, Dam inhibited CXCL12-induced chemotaxis in the 3–10 μM range in both Jurkat and JCaM1.6 cells (Figure 5, B and C). Because Lck is not expressed in JCaM1.6 cells, these results suggest that Dam inhibited CXCL12-induced chemotaxis not through the inhibition of Lck, but probably through the inhibition of LIMK1, at least in JCaM1.6 cells. To further address this issue, we next examined the effect of Dam on CXCL12-induced cofilin phosphorylation. As previously reported (Nishita *et al.*, 2002, 2005), the level of P-cofilin in Jurkat cells increased 5 min after CXCL12 stimulation, but this increase was suppressed after exposure of cells to 3–10 μM Dam (Figure 5D). By contrast, the increase in phosphorylated MAPK (P-MAPK) after CXCL12 stimulation was unaffected by Dam treatment (Figure 5D). These results suggest that Dam has the potential to inhibit CXCL12-induced LIMK1 activation and cofilin phosphorylation in Jurkat cells.

To further elucidate the mechanism by which Dam suppresses chemotactic migration of Jurkat cells, we analyzed changes in cell morphology and actin cytoskeleton by time-lapse fluorescence analysis. Jurkat cells expressing YFP-actin were treated with 3 μM Dam or control vehicle for 30 min and then stimulated with CXCL12. Before CXCL12 stimulation, the untreated control Jurkat cells exhibited a round cell morphology, but within 1–5 min of CXCL12 stimulation, there were multiple F-actin–rich lamellipodial protrusions around the circumference of the cell that were converted into a single lamellipodium on one side of the cell within 20 min (Figure 6A and Supplemental Movie S1). By contrast, Dam-treated cells formed only faint and immature lamellipodial protrusions before and after CXCL12 stimulation (Figure 6A and Supplemental Movie S2). Changes in cell morphology and actin cytoskeleton were also assessed using rhodamine–phalloidin staining before and 20 min after CXCL12 stimulation. Quantitative analysis confirmed that after CXCL12 stimulation, Dam-treated cells had fewer cells with large lamellipodial protrusions and more cells with small or no lamellipodial protrusions than the control cells (Figure 6B). The phenotypes of Dam-treated cells are similar to those of LIMK1-knockdown cells (Nishita *et al.*, 2005). Taken together, these findings suggest that Dam suppresses Jurkat cell migration by suppressing stimulus-induced F-actin assembly and the formation and maintenance of lamellipodial membrane protrusions, presumably by inhibiting the F-actin–stabilizing activity of LIMK1. Dam did not affect the cell morphology of non-stimulated cells, which suggests that LIMK1 is primarily involved in

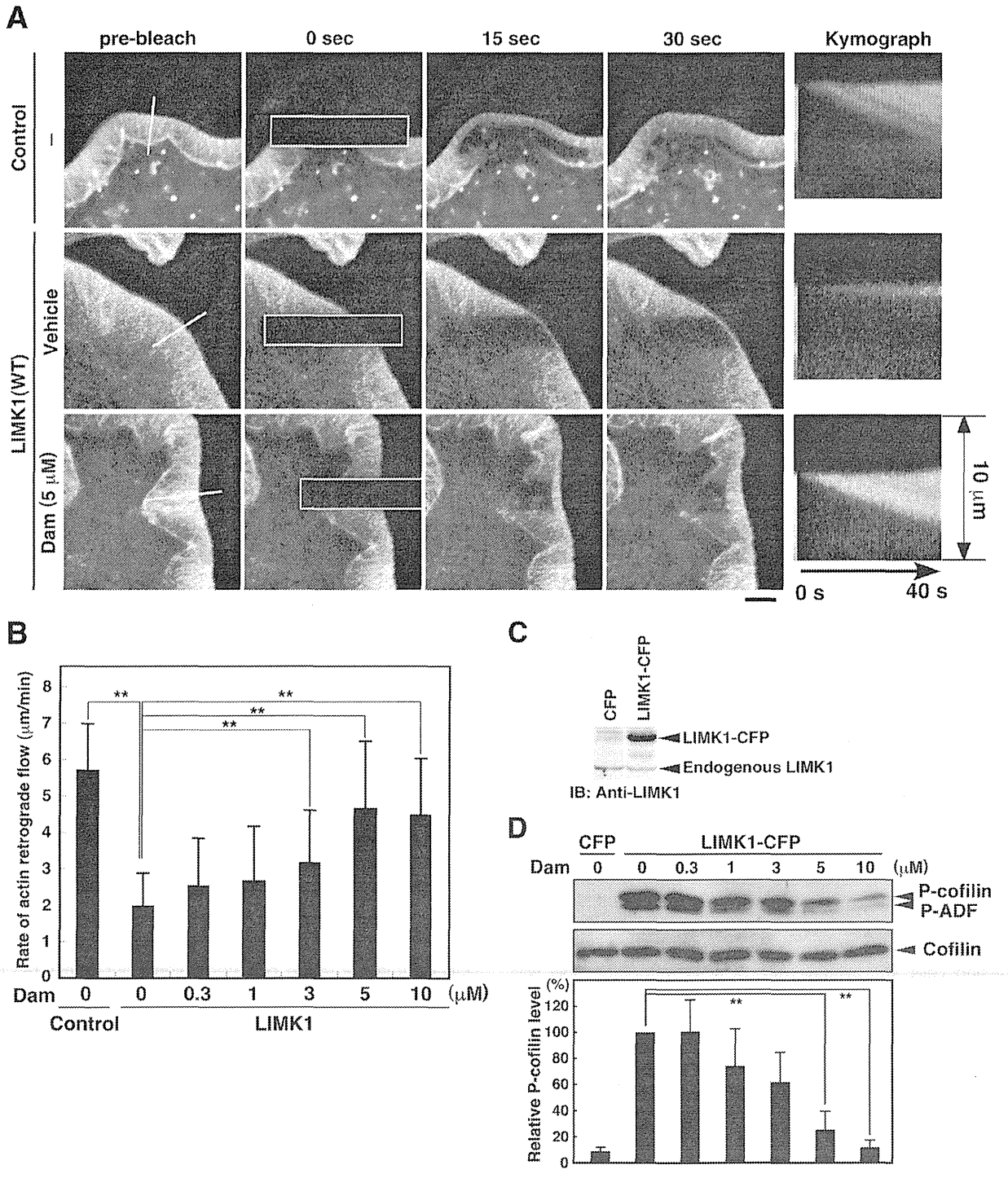

FIGURE 4: Dam inhibits LIMK1-induced deceleration of actin retrograde flow and cofilin phosphorylation. (A) FRAP time-lapse imaging of YFP-actin in RacV12-expressing N1E-115 cells. Cells were cotransfected with CFP (control) or CFP-LIMK1. Cells were pretreated with Dam or control vehicle (1% DMSO) for 30 min. After photobleaching of a rectangular region (white box), fluorescence images were acquired every 1 s for 40 s. Scale bar, 10 μm. Far right, kymographs of the white lined region (perpendicular to the cell margin) depicted at the far left. (B) Quantitative analysis of the effect of Dam on LIMK1-induced deceleration of the rate of actin retrograde flow in lamellipodia, measured by kymograph analysis. Data are mean values ± SD of three independent experiments. $^{**}p < 0.01$ by one-way ANOVA followed by Dunnett's test. (C) Level of LIMK1-CFP overexpression. N1E-115 cells were cotransfected with CFP (control) or LIMK1-CFP, and cell lysates were analyzed by immunoblotting with anti-LIMK1 antibody. (D) The effect of Dam on the level of cofilin phosphorylation. N1E-115 cells were cotransfected as before and treated with indicated concentrations of Dam for 30 min. Cell lysates were analyzed by immunoblotting with anti–P-cofilin and anti-cofilin antibodies. Bottom, relative P-cofilin levels, with the value in Dam-untreated, LIMK1-overexpressing cells taken as 100%. Data are mean values ± SD of three independent experiments. $^{**}p < 0.01$ by one-way ANOVA followed by Dunnett's test.

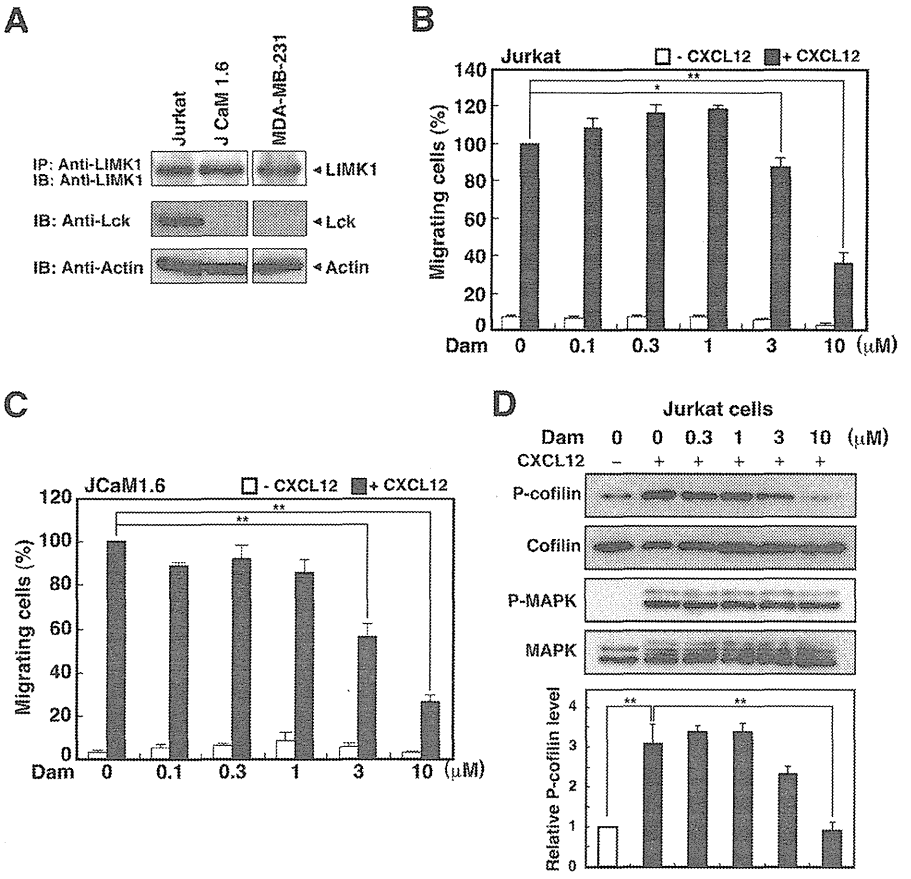

FIGURE 5: Dam inhibits chemotactic migration of Jurkat T-cells and Jurkat-derived, Lck-deficient JCaM1.6 cells. (A) Immunoblot analysis of the expression of LIMK1 and Lck in Jurkat, JCaM1.6, and MDA-MB-231 cells. Expression of Lck and control actin was analyzed by immunoblotting of cell lysates with anti-Lck and anti-actin antibodies. Expression of LIMK1 was analyzed by immunoprecipitation of cell lysates, followed by immunoblotting with anti-LIMK1 antibody. (B, C) Effect of Dam on CXCL12-induced chemotaxis of Jurkat (B) or JCaM1.6 (C) cells. Cells were pretreated with Dam and then loaded into the upper well of the Transwell chambers in the presence or absence of CXCL12 in the lower well. After incubation for 3 h, migrating cells in the lower well were counted. Data are mean values ± SD of four independent experiments. *$p < 0.05$, **$p < 0.01$, by one-way ANOVA followed by Dunnett's test. (D) Effect of Dam on CXCL12-induced cofilin phosphorylation in Jurkat cells. Cells were stimulated with 5 nM CXCL12 for 5 min and cell lysates analyzed by immunoblotting using antibodies to P-cofilin, cofilin, P-MAPK, and MAPK. Bottom, relative P-cofilin levels, with the value in control cells taken as 1.0. Data are mean values ± SD of three independent experiments. **$p < 0.01$ by one-way ANOVA followed by Dunnett's test.

stimulus-induced actin cytoskeletal remodeling and changes in cell morphology.

To further elucidate the pharmacological efficacy of Dam under various conditions, we analyzed the effect of washout on the inhibitory activity of Dam. Jurkat cells were treated with 5 μM Dam or control vehicle for 30 min and then washed three times with culture medium. Immediately or 30–180 min after washing, cells were stimulated with CXCL12 for 20 min and then fixed and stained with rhodamine–phalloidin, and the lamellipodium formation was analyzed as in Figure 6B. In accord with the result shown in Supplemental Figure S4B, washout of Dam before CXCL12 stimulation did not substantially affect the inhibitory activity of Dam on CXCL12-induced lamellipodium formation (Supplemental Figure S5, a–d), which suggests that Dam has the long-lasting inhibitory effect, presumably by forming a stable adduct with the target kinase. In addition, application of Dam immediately after CXCL12 stimulation inhibited CXCL12-induced lamellipodium formation, but application of Dam 10 min after CXCL12 stimulation reduced the inhibitory effect of Dam on CXCL12-induced large lamellipodium formation (Supplemental Figure S5, a, e, and g), which suggests that Dam inhibits CXCL12-induced lamellipodium formation by predominantly inhibiting the early step (occurring within 10 min after cell stimulation) of lamellipodium formation.

Dam inhibits migration and invasion of MDA-MB-231 breast carcinoma cells

Several lines of evidence show that LIMK1 is required for tumor cell migration and invasion (Yoshioka *et al.*, 2003; Horita *et al.*, 2008; Mishima *et al.*, 2010). Because MDA-MB-231 human breast carcinoma cells are known to express LIMK1 and require it for cell migration and invasion (Scott *et al.*, 2010), we investigated the effect of Dam on serum-induced chemotactic migration and invasion of MDA-MB-231 cells. Immunoblot analysis revealed that LIMK1, but not Lck, is expressed in MDA-MB-231 cells (Figure 5A). Serum-induced chemotactic migration of MDA-MB-231 cells was significantly suppressed by exposure of cells to 1–10 μM Dam (Figure 7A). To examine the effect of Dam on the invasive activity of MDA-MB-231 cells, we loaded the cells on Matrigel in the upper chamber of Transwell chambers and added serum to the lower chamber. After incubation for 15 h, the cells that had invaded in the lower chamber were counted. Serum-induced invasion of MDA-MB-231 cells was significantly suppressed by exposing the cells to 3–10 μM Dam (Figure 7B). Thus Dam is a potent inhibitor of migration and invasion of MDA-MB-231 breast carcinoma cells.

Topical application of Dam inhibits hapten-stimulated migration of epidermal Langerhans cells in mouse ears

The epidermal Langerhans cell is a member of the dendritic cell family, and it initiates cutaneous immune responses by transporting foreign antigen for presentation to T lymphocytes in the skin-draining lymph nodes. To do this, the cells migrate from the epidermis to draining lymph nodes in response to chemical allergens on the skin surface (Cumberbatch *et al.*, 2000). To examine whether Dam affects cell migration in vivo, we analyzed the effect of topical administration of Dam on hapten-stimulated migration of epidermal Langerhans cells in mouse ears. Mouse ears were painted with 3% (wt/vol) 2,4,6-trinitrochlorobenzene (TNCB) in acetone/olive oil (1:4) or vehicle (acetone/olive oil) alone as a control. After 24 h of TNCB exposure, the epidermal sheets were prepared from the ear skins and stained with fluorescein isothiocyanate (FITC)–labeled anti-mouse

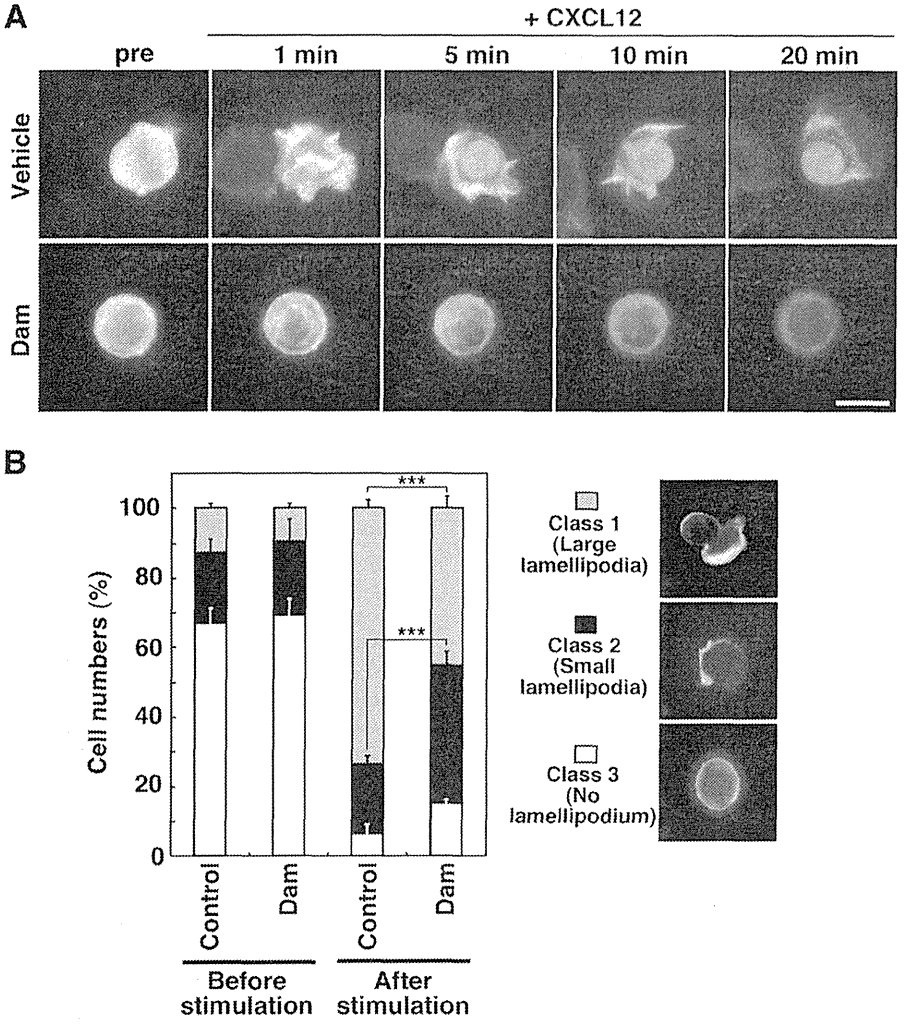

FIGURE 6: Effect of Dam on CXCL12-induced F-actin assembly and membrane protrusion formation in Jurkat cells. (A) Time-lapse fluorescence analysis. Jurkat cells transfected with YFP-actin were treated with 5 μM Dam or control vehicle (0.1% DMSO) for 30 min and then stimulated with 5 nM CXCL12 for 20 min. The levels of F-actin assembly and membrane protrusion were analyzed by time-lapse analysis of YFP fluorescence. Scale bar, 10 μm. See also Supplemental Movies S1 and S2. (B) The effect of Dam on the lamellipodium formation of Jurkat cells before and after CXCL12 stimulation. Cells were treated with 5 μM Dam or control vehicle for 30 min and then stimulated with 5 nM CXCL12 for 20 min. Cells were fixed and stained with rhodamine–phalloidin to detect F-actin and categorized into three classes: 1, cells with large lamellipodia; 2, cells with small lamellipodia; 3, round cells without a lamellipodium. Percentages of cells in each class are shown as mean values ± SD of three independent experiments (200–300 cells were counted in each experiment). ***$p < 0.005$ by Student's t test.

I-Ad monoclonal antibody to visualize class II MHC in epidermal Langerhans cells on the ear epidermis (Aiba and Katz, 1990). Treatment with TNCB significantly decreased the density of Langerhans cells on the ear epidermis (Figure 8, A–C and F), indicating that TNCB administration induced migration of epidermal Langerhans cells to the lymph nodes. To examine the effect of Dam on in vivo cell migration, Dam (20 μM) or vehicle solution was topically applied on the ear skin 30 min before, immediately after, and 12 h after TNCB painting. The density of Langerhans cells was analyzed as before, and in the TNCB-administrated ear epidermis, it was found to be significantly higher in Dam-treated mouse ears compared with vehicle treatment (Figure 8, C, E, and F), whereas Dam treatment of control ears had no effect on Langerhans cell density (Figure 8, D and F). These results indicate that Dam has the potential to suppress hapten-induced migration of epidermal Langerhans cells. Further studies are required to determine whether Dam suppressed Langerhans cell migration via LIMK1 inhibition. On hapten stimulation, Langerhans cells appeared to increase cell size, as reported (Aiba and Katz, 1990; Kubo *et al.*, 2009), but Dam treatment had no apparent effect on the cell size changes (Figure 8, C and E).

DISCUSSION

In this study, two compounds, Dam and MO-26, were identified as effective inhibitors of LIMKs. Both were previously reported to be effective inhibitors of Lck tyrosine kinase (Faltynek *et al.*, 1995; Burchat *et al.*, 2002). Despite the different backbone structures (Dam is an anthraquinone derivative, whereas MO-26 is a pyrrazolopyrimidine derivative), both exhibited effective inhibition of LIMKs and Lck, with no apparent effect on ROCK, PAK3, PKCα, and CaMKIα. However, Dam is a better inhibitor of LIMK1, whereas MO-26 is a better inhibitor of Lck. Although LIMKs are known to phosphorylate the Ser-3 residue of cofilin/ADF family proteins, they share sequence similarities with tyrosine kinases and possess unique sequence motifs, such as DLNSHN in the VIB subdomain of the kinase catalytic domain (Okano *et al.*, 1995; Manning *et al.*, 2002). In addition, unpublished results from this lab indicate that LIMK1 has weak tyrosine kinase activity. These results suggest that the active-site tertiary structures of LIMKs and Lck are sufficiently similar to allow binding and inhibition by Dam and MO-26. Although several inhibitors of Lck (Meyn and Smithgall, 2008) and LIMKs (Ross-Macdonald *et al.*, 2008; Harrison *et al.*, 2009; Prudent *et al.*, 2012; Manetti, 2012a) have been reported, in light of the results presented here, it is clear that there is potential for cross-specificity of inhibition; hence it is important to reexamine whether these compounds are indeed specific for each of these kinases. Moreover, it is important to determine the target specificity of Dam and MO-26 more precisely by using comprehensive kinase profiling. Research from this lab is focused on the development of more-selective LIMK inhibitors, using Dam and MO-26 as lead compounds.

Based on the results that Dam inhibits Lck and suppresses CXCL12-induced migration of Jurkat cells, it was postulated that Lck plays a crucial role in T-cell chemotaxis (Inngjerdingen *et al.*, 2002). In this study, Dam suppressed CXCL12-induced chemotactic migration in both Jurkat and Jurkat-derived, Lck-deficient JCaM1.6 cells. Dam also caused inhibition of CXCL12-induced cofilin phosphorylation and chemotactic migration of Jurkat cells in a similar dose-dependent manner. Moreover, we previously showed that LIMK1 knockdown suppresses CXCL12-induced chemotaxis of Jurkat cells (Nishita *et al.*, 2002, 2005). Together these results suggest that Dam suppresses T-cell chemotaxis primarily by inhibiting LIMK1, at

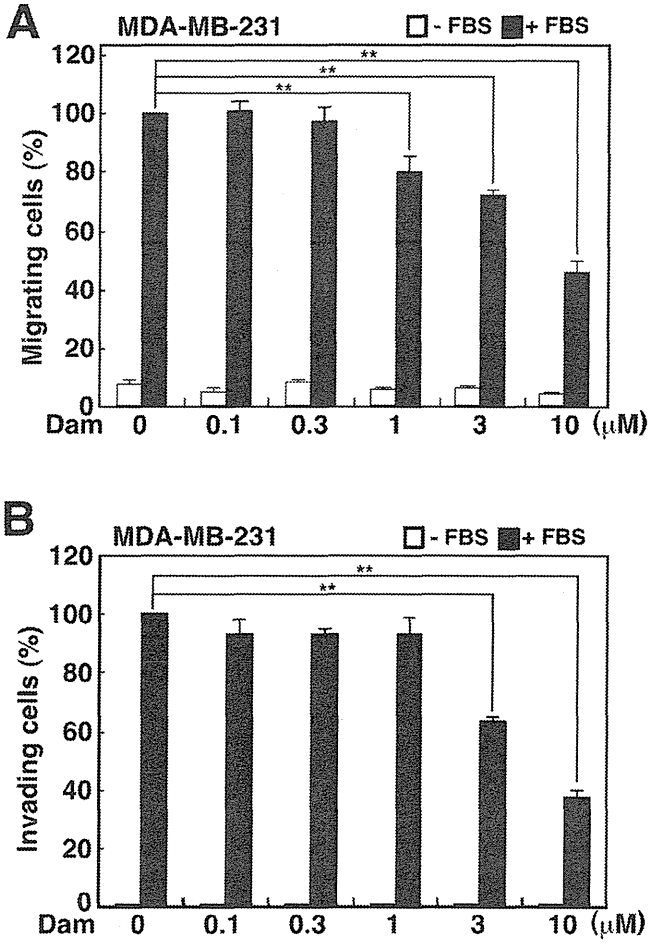

FIGURE 7: Dam inhibits migration and invasion of MDA-MB-231 breast carcinoma cells. (A) Migration assay. Cells were incubated with indicated concentrations of Dam or vehicle for 30 min and loaded into the upper well of the Transwell chambers in the presence or absence of 10% FCS in the lower well. After a 3-h incubation, the migrating cells on the lower face of the membrane were counted. (B) Invasion assay. Matrigel was placed onto the upper well of the Transwell chambers, cells were loaded onto Matrigel and cultured for 15 h, and the invading cells on the lower face of the membrane were counted. Data are mean values ± SD of four (A) or six (B) independent experiments. $^{**}p < 0.01$ by one-way ANOVA followed by Dunnett's test.

least in Lck-deficient JCaM1.6 cells. As for Jurkat cells, the possibility cannot be excluded that Dam may suppress migration through inhibition of both LIMK1 and Lck. Treatment with Dam suppressed CXCL12-induced lamellipodium formation in Jurkat cells, with a similar phenotype to that of LIMK1 knockdown cells (Nishita *et al.*, 2005), which indicates that LIMK1 plays a critical role in Jurkat cell migration by promoting stimulus-induced lamellipodium formation.

Dam also suppressed migration and invasion of MDA-MB-231 breast carcinoma cells, which have no detectable expression of Lck, further supporting the hypothesis that Dam suppresses MDA-MB-231 cell migration and invasion primarily through inhibition of LIMKs. Previous studies demonstrated the crucial role of LIMKs in tumor cell invasion and metastasis (Davila *et al.*, 2003; Yoshioka *et al.*, 2003; Wang *et al.*, 2007; Horita *et al.*, 2008; Mishima *et al.*, 2010; Scott *et al.*, 2010). Thus Dam could be used to develop a therapeutic agent against LIMK-mediated tumor cell invasion and metastasis.

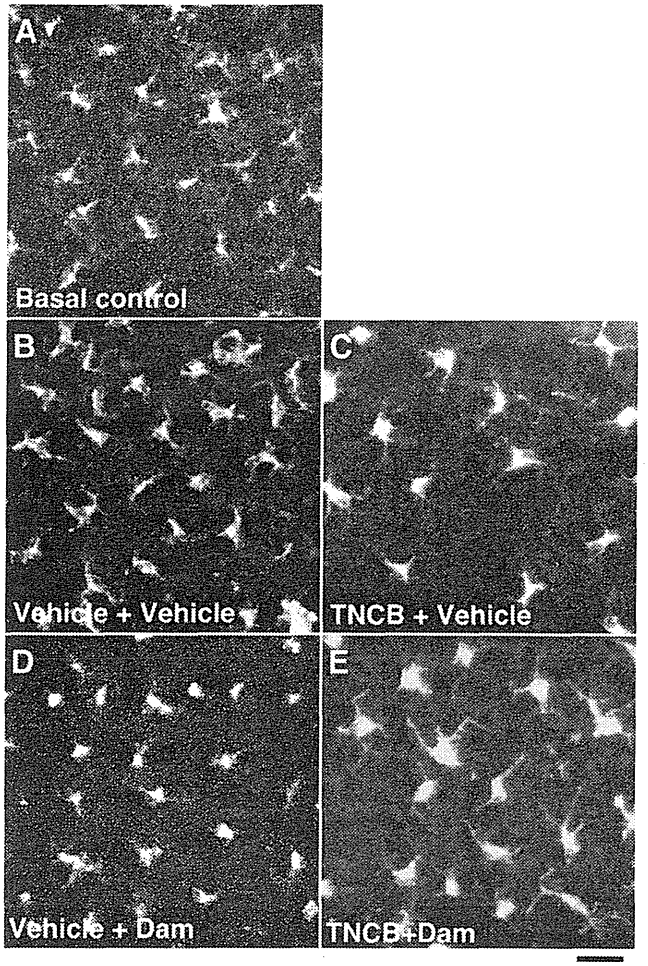

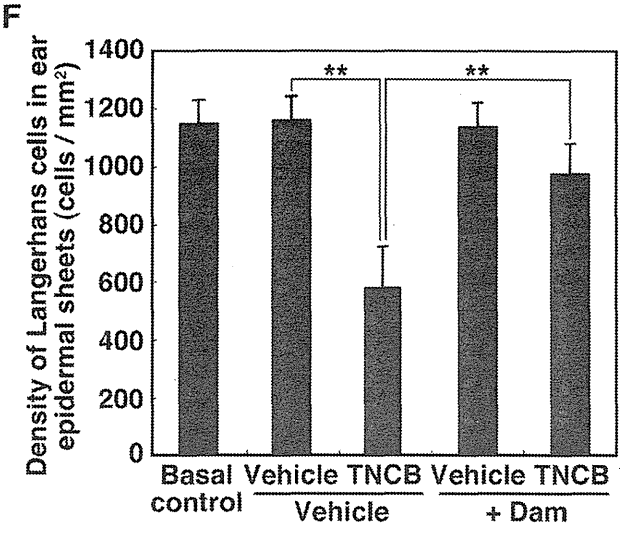

FIGURE 8: Topical application of Dam inhibits hapten-induced migration of epidermal Langerhans cells in mouse ears. (A) Direct immunofluorescence analysis of epidermal sheets, using FITC-labeled anti-mouse I-Ad monoclonal antibody. Epidermal sheets were obtained from normal skin (A) or skin painted with vehicle (B), TNCB (C), Dam (D), or TNCB and Dam (E). Scale bar, 20 μm. (F) Quantitative analysis of density of Langerhans cells in ear epidermal sheets. Data are mean values ± SD of five independent experiments (cell density was analyzed in 15 areas/mouse ear in each experiment). $^{**}p < 0.01$ by one-way ANOVA followed by Dunnett's test.

In this study, topical application of Dam impaired hapten-induced migration of epidermal Langerhans cells in the mouse ear. Langerhans cells in the epidermis play a central role in the initiation and elicitation of cutaneous immune responses and the pathogenesis of allergic contact dermatitis. Langerhans cells recognize, internalize, and process the antigens and carry them from the epidermis to draining lymph nodes, where they are presented to antigen-responsive T-lymphocytes that drive primary immune responses (Cumberbatch *et al.*, 2000; Kimber *et al.*, 2000). Inhibition of Langerhans cell migration could be a promising strategy to alleviate allergic skin diseases, such as contact hypersensitivity and atopic dermatitis. Topical treatment with Dam suppressed this migration; hence Dam could be a suitable starting point for the development of agents against allergic inflammatory diseases.

LIMKs are key regulators of actin cytoskeletal reorganization through the phosphorylation and inactivation of cofilin. They play essential roles in diverse cell functions, including cell migration, morphogenesis, division, polarity formation, gene expression, neurite outgrowth, and cancer cell invasion (Scott and Olson, 2007; Mizuno, 2013). Identification of Dam and MO-26 as effective LIMK inhibitors provides a useful tool for investigating the functional roles of LIMKs in cellular and pathophysiological processes. Aberrant regulation of LIMK activity has been reported to be involved in the pathogenesis of cancer metastasis and cardiovascular and neurological disorders (Scott and Olson, 2007; Manetti, 2012a; Mizuno, 2013), and LIMK2 inhibitors have been used to treat ocular hypertension and associated glaucoma in model animals (Harrison *et al.*, 2009). Thus LIMKs are promising therapeutic targets, and specific inhibitors of LIMKs are attractive candidates for novel therapeutic drugs against these diseases.

This study applied a new BiFC assay system recently developed in our laboratory to screen for LIMK1 inhibitors (Ohashi *et al.*, 2012). The assay, which uses a pair of Venus fragments obtained by splitting the Venus fluorescent protein at position 210, can quantitatively measure protein–protein interactions with high specificity and low background fluorescence. Recently it was successfully used to screen for inhibitors that block protein–protein interactions (Shoji *et al.*, 2012). Therefore, the BiFC assay system will provide a useful method for screening inhibitors of various protein kinases, once the BiFC probes that properly detect the phosphorylation-dependent protein–protein interactions can be developed. Protein phosphorylation can negatively and positively regulate protein–protein interactions. For example, as reported here, LIMK1-mediated cofilin phosphorylation negatively regulated the actin–cofilin interaction. Conversely, protein phosphorylation by PKB/Akt or PKD often produces the binding site for 14-3-3 proteins in target proteins (Tzivion and Avruch, 2002), and the cross-phosphorylation of receptor tyrosine kinases produces the binding sites for Src homology region 2 domain–containing or phosphotyrosine-binding domain–containing proteins in receptor proteins (Schlessinger and Lemmon, 2003). Thus it is feasible to develop the BiFC assay system to screen for inhibitors of these protein kinases. Targeted inhibition of protein kinases is considered to be a promising therapeutic strategy in the treatment of relevant diseases (Cohen, 2002). Based on an approach similar to that outlined in this study, the BiFC assay system will provide a useful method for identifying new inhibitors of protein kinases and facilitating the development of attractive therapeutic drugs that target specific protein kinases.

MATERIALS AND METHODS

Materials

SCADS inhibitor kits I and II (each consisting of 95 chemical inhibitors) were provided by the Screening Committee of Anticancer Drugs via a Grant-in-Aid for Scientific Research (priority area "Cancer") from the Ministry of Education, Culture, Sports, Science and Technology, Japan. Other chemical compounds (MO-1 to MO-768) were synthesized as partial structures and analogues of natural products, as well as of enzyme inhibitors (Oikawa *et al.*, 1995, 2005; Kusumoto and Oikawa, 2001; Oikawa, 2010). Dam (Enzo Life Sciences, Farmingdale, NY), emodin (Tokyo Chemical Industry, Tokyo, Japan), and mitoxantrone (Sigma-Aldrich, St. Louis, MO) were purchased commercially. CXCL12 was purchased from PeproTech (Rocky Hill, NJ). Rabbit polyclonal antibodies against LIMK1, cofilin, and P-cofilin were generated as described (Okano *et al.*, 1995; Toshima *et al.*, 2001). Mouse monoclonal antibody against Myc epitope (9E10) and rat monoclonal antibody against hemagglutinin epitope (3F10) were purchased from Roche Diagnostics (Basel, Switzerland). Mouse monoclonal antibodies against Lck (3A5) and Src (B-12) were purchased from Santa Cruz Biotechnology (Santa Cruz, CA). Mouse monoclonal antibodies against MAPK, P-MAPK, and β-actin (AC-15) were purchased from Sigma-Aldrich. FITC-labeled anti-mouse I-Ad antibody was purchased from BioLegend (San Diego, CA).

Plasmid construction

Venus cDNA was provided by A. Miyawaki (Riken, Wako, Japan; Nagai *et al.*, 2002). The cDNA plasmids for LIMK1 and LIMK2 were constructed as described previously (Mizuno *et al.*, 1994; Okano *et al.*, 1995). The cDNA plasmids for GST-ROCKΔ3 (amino acids 1–727) and PAKΔN (amino acids 162–544) were provided by S. Narumiya (Kyoto University, Kyoto, Japan) and H. Sumimoto (Kyushu University, Fukuoka, Japan), respectively. The cDNA plasmids for mouse Lck and human Src were purchased from Open Biosystems (Tokyo, Japan). The cDNA plasmids for PKCα and CaMKIα were constructed by PCR amplification. For the in vitro BiFC assays, expression plasmids for actin-VC210-His_6, VN210-cofilin-His_6, LIMK1-(Myc+His), and GST-ROCKΔ3 were constructed by inserting the cDNAs into the pFastBac1 baculovirus expression vector (Invitrogen, Carlsbad, CA; Ohashi *et al.*, 2012). For the in vitro kinase assays, expression plasmids for (Myc+His)-tagged LIMK1, LIMK2, Lck, SrcΔC (amino acids 1–322), ROCKΔ3, and PAK3ΔN and HA-tagged PKCα were constructed by inserting the cDNAs into the pcDNA3.1/(Myc+His) (Invitrogen)– or pEYFP-C1 (Clontech, Mountain View, CA)–derived pHA-C1 vector. Expression plasmids coding for the kinase-dead mutants were constructed using a site-directed mutagenesis kit (Stratagene, Santa Clara, CA). Expression plasmids for GFP-CaMKIα-(1-293) and -(K49E) were constructed as described previously (Saito *et al.*, 2013). Expression plasmids for YFP-actin, HA-RacV12, and CFP-tagged LIMK1 were constructed as described previously (Ohashi *et al.*, 2011).

Cell culture and transfection

N1E-115, COS-7, and MDA-MB-231 cells were cultured in DMEM supplemented with 10% (vol/vol) fetal calf serum (FCS). These cells were transfected with plasmids using Lipofectamine 2000 (Invitrogen). Jurkat and JCaM1.6 cells were cultured in RPMI medium supplemented with 10% (vol/vol) FCS. Jurkat cells were transfected by electroporation at 280 V and 975 μF using a Gene Pulser II (Bio-Rad, Hercules, CA), as described previously (Nishita *et al.*, 2005).

LIMK1 inhibitor screens

Screening of LIMK1 inhibitors was performed using the in vitro BiFC assay with probes composed of actin-VC210 and VN210-cofilin, as described previously (Ohashi *et al.*, 2012). His_6-tagged actin-VC210, VN210-cofilin, and LIMK1-(Myc+His) were expressed in Sf9 or Sf21

cells, using the Bac-to-Bac baculovirus expression system (Invitrogen). Proteins were resolved on a nickel-nitrilotriacetic acid agarose (Qiagen, Valencia, CA) column and eluted with 0.2 M imidazole buffer, and the elution buffer containing each protein was exchanged for binding buffer using a PD-10 gel-filtration column (GE Healthcare, Piscataway, NJ; Ohashi *et al.*, 2012). GST-ROCKΔ3 was expressed in Sf21 cells, purified using a glutathione–Sepharose (GE Healthcare) column, and eluted with glutathione buffer, and the elution buffer containing GST-ROCKΔ3 was exchanged using a PD-10 column. LIMK1 was incubated with ROCKΔ3 and ATP at 30°C for 10 min and then with one of the small organic compounds at a final concentration of 6.6 μM for known inhibitors or 10 μM for synthetic compounds in 30 μl of screening buffer (40 mM Tris-HCl, pH 7.4, 1 mM ATP, 100 mM NaCl, 2 mM $MgCl_2$, 1 mM dithiothreitol) in 96-well microtiter plates. Chemical compounds were used after dissolving in dimethylsulfoxide (DMSO). After incubation for 5 min, the VN210-cofilin probe (3 μM) was added to the mixture and incubated at 30°C for 1 h. Then actin-VC210 (1.5 μM) was added and fluorescence intensity was measured at 0 and 120 min at 545 nm with excitation at 505 nm in a fluorescence microphotometer. Experiments were carried out in duplicate, and recovery of fluorescence intensity was calculated relative to control (in the absence of compound).

In vitro kinase assay

COS-7 cells were transfected with cDNA plasmids coding for LIMK1-Myc, LIMK2-Myc, Src-(Myc+His), Lck-(Myc+His), ROCK-Myc, PAK3-Myc, HA-PKCα, GFP-CaMKIα, or their mutants using Lipofectamine 2000 (Invitrogen). After 48 h, cells were washed with phosphate-buffered saline (PBS) and lysed by resuspension in lysis/kinase buffer (50 mM 4-(2-hydroxyethyl)-1-piperazineethanesulfonic acid [HEPES], pH 7.4, 150 mM NaCl, 0.5% [vol/vol] Nonidet P-40, 5% [vol/vol] glycerol, 1 mM $MgCl_2$, 1 mM $MnCl_2$, 10 mM NaF, 1 mM Na_3VO_4, 1 mM dithiothreitol, 1 mM phenylmethylsulfonyl fluoride, and 10 μg/ml leupeptin). After centrifugation to remove debris, supernatants were incubated for 4 h at 4°C with anti-Myc, anti-HA, or anti-GFP antibody and protein A–Sepharose (GE Healthcare). The immunoprecipitates were washed three times with the lysis/kinase buffer and subjected to an in vitro kinase reaction. In vitro kinase reactions were performed in 20 μl of lysis/kinase buffer containing 100 μM ATP and 185 kBq of [γ-^{32}P]ATP (110 TBq/mmol), supplemented with 2 μg of substrate (either recombinant cofilin or MBP), in the presence or absence of chemical inhibitors (Dam or MO-26 in 1 μl of DMSO) at 30°C for 40 min. The reaction mixture was boiled in SDS sampling buffer, and aliquots were separated by SDS–PAGE. Proteins were transferred to polyvinylidene fluoride membranes and analyzed by autoradiography using BAS1000 Bio-image analyzer (Fuji Film, Tokyo, Japan), amido black staining, and immunoblotting with anti-Myc, anti-HA, or anti-GFP antibody. Kinase activity was measured via ^{32}P incorporation into the substrate protein and expressed as relative activity using control activity, in the absence of inhibitor, as 100%. The IC_{50} values were calculated using Prism software (GraphPad, La Jolla, CA).

Measurement of the rate of actin retrograde flow using FRAP time-lapse imaging

N1E-115 cells were cotransfected with the cDNA plasmids for YFP-actin, Rac-V12, and LIMK1-CFP or control vector and cultured for 24 h. Cells were pretreated with Dam or the control (drug vehicle, 1% [vol/vol] DMSO) at 37°C for 30 min and then subjected to FRAP time-lapse assays. FRAP analysis was performed using a laser-scanning confocal microscope (LSM 510; Carl Zeiss, Jena, Germany) equipped with a PL Apo 63× oil-immersion objective lens (numerical aperture 1.4), as described previously (Ohashi *et al.*, 2011). N1E-115 cells were plated on a 35-mm glass-bottom dish and maintained in DMEM containing 10 mM HEPES, pH 7.4, and 10% FCS, at 37°C in a heat insulation chamber. Before photobleaching, a fluorescence image of the cell in a rectangular region (512 × 300 pixels) was acquired by irradiation with 0.5–1% of power from a 514-nm argon-ion laser. Photobleaching was performed in a rectangular region (45 × 225 pixels, 101 μm^2) of partially overlapping lamellipodium by 30 times irradiation for a total time of 3.1 s with full power of a 30-mW argon-ion laser at 458, 488, and 514 nm. Immediately after photobleaching, fluorescence images of the foregoing cell areas were acquired every second for 30 s by weak irradiation with a 514-nm argon-ion laser. The rate of actin retrograde flow was measured by kymograph analysis. Kymograph analysis was conducted with a customized macro in ImageJ (http://rsb.info.nih.gov/ij/). The kymograph image was constructed using stacked images of 3 × 100–pixel (0.3 × 10 μm) areas, which were taken by FRAP time-lapse analysis. The rate of actin retrograde flow was measured as the rate at which the boundary between the bright and dark areas of the recovering YFP-actin fluorescence signal migrated inward from the initial cell margin.

Time-lapse fluorescence imaging to detect changes in actin organization in Jurkat cells

For time-lapse imaging, Jurkat cells were electroporated with plasmids coding for YFP-actin. Images of stacked optical sections were collected every 30 s for 20 min after CXCL12 stimulation using a laser-scanning confocal microscope and objective lens, as described previously (Nishita *et al.*, 2005).

Cell migration and invasion assays

Jurkat or JCaM1.6 cells (2 × 10^6 cells/ml) were resuspended in RPMI1640 medium containing 0.5% bovine serum albumin (BSA) and pretreated with Dam or drug vehicle (final concentration 0.3% [vol/vol] DMSO) for 30 min at room temperature. Cells (2 × 10^5 cells) in 100 μl of medium were loaded into the upper well of the 24-well Transwell culture chamber (5-μm pore size; Corning, Lowell, MA), and 400 μl of RPMI medium containing 0.5% BSA, 5 nM CXCL12, and Dam or vehicle (final 0.3% DMSO) was added to the lower well. After incubation for 3 h at 37°C, the cells that had migrated into the lower well were counted. MDA-MB-231 cells (2 × 10^5 cells/ml) were serum starved for 3 h, resuspended in serum-free DMEM, and pretreated with Dam or vehicle (final 0.3% DMSO) for 30 min at room temperature. Aliquots of cells (2 × 10^4 cells) in 100 μl of medium were loaded into the upper well of Transwell chambers (8-μm pore size). The lower wells were filled with 400 μl of DMEM containing 10% FCS and Dam or vehicle (final 0.3% DMSO). After incubation for 3 h at 37°C, cells were fixed with 3.7% formaldehyde and stained with 4′,6-diamidino-2-phenylindole. The nonmigrating cells on the top of the membrane were gently removed by wiping and rinsing, and the migrating cells on the lower face of the membrane were counted. For invasion assays, 50 μg/50 μl of Matrigel (Becton-Dickinson, San Diego, CA) were loaded into the upper well of Transwell chambers (8-μm pore size) and incubated for 1 h at 37°C. After washing the Matrigel with DMEM three times, MDA-MB-231 cells (2 × 10^4 cells) were loaded onto Matrigel and cultured for 15 h, and the cells invading on the lower face of the membrane were counted, as described.

Immunoprecipitation and immunoblot analysis

Cells were lysed with lysis/kinase buffer, and the lysates were subjected to immunoprecipitation or immunoblot analyses, as described previously (Okano *et al.*, 1995).

In vivo migration assays of epidermal Langerhans cells

BALB/c mice at age 8–10 wk were painted on the ears with 20 µl of 20 µM Dam in 2% DMSO or vehicle (2% DMSO) in 1:4 (vol/vol) acetone/olive oil. After 30 min, the ears were painted with 20 µl of 3% (wt/vol) TNCB in 1:4 (vol/vol) acetone/olive oil or vehicle (acetone/olive oil) with or without 20 µM Dam. After 12 h, the ears were painted again with 20 µl of 20 µM Dam in 2% DMSO or control vehicle. Control and TNCB-painted ear skins were obtained 24 h after TNCB painting. Using standard techniques, epidermal sheet preparations were made and stained with a monoclonal antibody with specificity for I-Ad (Caughman *et al.*, 1986; Aiba and Katz, 1990). Epidermal sheets were obtained after incubation in 0.5 M NH_4SCN at 37°C for 30 min. The sheets were fixed in acetone for 10 min and blocked with PBS containing 0.2% (wt/vol) bovine serum albumin and 0.02% (wt/vol) sodium azide. After incubation with FITC-labeled anti-mouse I-Ad monoclonal antibody (BioLegend) for 3 h, the sheets were washed with PBS, mounted with nonfluorescent glycerol, and analyzed using confocal fluorescence microscopy.

Statistical analysis

Statistical data are expressed as the means ± SD of more than three independent experiments. All statistical analyses were performed by Prism 6 (GraphPad). The p values were calculated using unpaired two-tailed Student's t test for pairwise data comparisons (in Figure 6 and Supplemental Figure S5) or one-way analysis of variance (ANOVA) followed by Dunnett's test for multiple data set comparison (in Figures 4, 5, 7, and 8 and Supplemental Figure S4). $p < 0.05$ was considered to be significant.

ACKNOWLEDGMENTS

We thank A. Miyawaki for providing Venus cDNAs, S. Narumiya for providing GST-ROCKΔ3 cDNA, H. Sumimoto for providing PAKΔN cDNA, and T. Yamori, the Head of the Screening Committee of Anticancer Drugs, for supplying the SCADS inhibitor kits. We also thank K. Shoji, T. Kiuchi, S. Fujiwara, Y. Ohta, K. Kitatani, and A. Saito for technical assistance. This work was supported by Grants-in-Aid for Scientific Research from the Ministry of Education, Culture, Science, Sports and Technology of Japan (23112005 and 25440076 to K.O. and 24121702 and 24370051 to K.M.) and Research Grants from the Mitsubishi Foundation (to K.M.) and the Uehara Memorial Foundation (to K.M.).

REFERENCES

Aiba S, Katz SI (1990). Phenotypic and functional characteristics of in vivo-activated Langerhans cells. J Immunol 145, 2791–2796.

Amano T, Tanabe K, Eto T, Narumiya S, Mizuno K (2001). LIM-kinase 2 induces formation of stress fibres, focal adhesions and membrane blebs, dependent on its activation by Rho-associated kinase-catalysed phosphorylation at threonine-505. Biochem J 354, 149–159.

Arber S, Barbayannis FA, Hanser H, Schneider C, Stanyon CA, Bernard O, Caroni P (1998). Regulation of actin dynamics through phosphorylation of cofilin by LIM-kinase. Nature 393, 805–809.

Bamburg JR, Wiggan OP (2002). ADF/cofilin and actin dynamics in disease. Trends Cell Biol 12, 598–605.

Borhani DW, Calderwood DJ, Friedman MM, Hirst GC, Li B, Leung AK, McRae B, Ratnofsky S, Ritter K, Waegell W (2004). A-420983: a potent, orally active inhibitor of lck with efficacy in a model of transplant rejection. Bioorg Med Chem Lett 14, 2613–2616.

Bravo-Cordero JJ, Magalhaes MA, Eddy RJ, Hodgson L, Condeelis J (2013). Functions of cofilin in cell locomotion and invasion. Nat Rev Mol Cell Biol 14, 405–415.

Burchat AF, Calderwood DJ, Friedman MM, Hirst GC, Li B, Rafferty P, Ritter K, Skinner BS (2002). Pyrazolo[3,4-d]pyrimidines containing an extended 3-substituent as potent inhibitors of Lck—a selectivity insight. Bioorg Med Chem Lett 12, 1687–1690.

Caughman SW, Sharrow SO, Shimada S, Stephany D, Mizuochi T, Rosenberg AS, Katz SI, Singer A (1986). Ia+ murine epidermal Langerhans cells are deficient in surface expression of the class I major histocompatibility complex. Proc Natl Acad Sci USA 83, 7438–7442.

Cohen P (2002). Protein kinases—the major drug targets of the twenty-first century. Nat Rev Drug Discov 1, 309–315.

Cumberbatch M, Dearman RJ, Griffiths CE, Kimber I (2000). Langerhans cell migration. Clin Exp Dermatol 25, 413–418.

Davila M, Frost AR, Grizzle WE, Chakrabarti R (2003). LIM kinase 1 is essential for the invasive growth of prostate epithelial cells: implications in prostate cancer. J Biol Chem 278, 36868–36875.

Edwards DC, Sanders LC, Bokoch GM, Gill GN (1999). Activation of LIM-kinase by Pak1 couples Rac/Cdc42 GTPase signalling to actin cytoskeletal dynamics. Nat Cell Biol 1, 253–259.

Faltynek CR *et al.* (1995). Inhibition of T lymphocyte activation by a novel p56lck tyrosine kinase inhibitor. J. Enzyme Inhib 9, 111–122.

Harrison BA *et al.* (2009). Novel class of LIM-kinase 2 inhibitors for the treatment of ocular hypertension and associated glaucoma. J Med Chem 52, 6515–6518.

Horita Y, Ohashi K, Mukai M, Inoue M, Mizuno K (2008). Suppression of the invasive capacity of rat ascites hepatoma cells by knockdown of Slingshot or LIM kinase. J Biol Chem 283, 6013–6021.

Inngjerdingen M, Torgersen KM, Maghazachi AA (2002). Lck is required for stromal cell-derived factor 1 alpha (CXCL12)-induced lymphoid cell chemotaxis. Blood 99, 4318–4325.

Jayasuriya H, Koonchanok NM, Geahlen RL, McLaughlin JL, Chang CJ (1992). Emodin, a protein tyrosine kinase inhibitor from *Polygonum cuspidatum*. J Nat Prod 55, 696–698.

Kerppola TK (2009). Visualization of molecular interactions using bimolecular fluorescence complementation analysis: characteristics of protein fragment complementation. Chem Soc Rev 38, 2876–2886.

Kimber I, Cumberbatch M, Dearman RJ, Bhushan M, Griffiths CE (2000). Cytokines and chemokines in the initiation and regulation of epidermal Langerhans cell mobilization. Br J Dermatol 142, 401–412.

Kubo A, Nagao K, Yokouchi M, Sasaki H, Amagai M (2009). External antigen uptake by Langerhans cells with reorganization of epidermal tight junction barriers. J Exp Med 206, 2937–2946.

Kusumoto S, Oikawa M (2001). Synthesis of glycolipid targets. In: Glycoscience. Chemistry and Chemical Biology I–III, ed. BO Fraser-Reid, K Tatsuta, and J Thiem, Heidelberg, Germany: Springer, 2107–2148.

Manetti F (2012a). LIM kinases are attractive targets with many macromolecular partners and only a few small molecule regulators. Med Res Rev 32, 968–998.

Manetti F (2012b). Recent findings confirm LIM domain kinases as emerging target candidates for cancer therapy. Curr Cancer Drug Targets 12, 543–560.

Manning G, Whyte DB, Martinez R, Hunter T, Sudarsanam S (2002). The protein kinase complement of the human genome. Science 298, 1912–1934.

Meberg PJ, Ono S, Minamide LS, Takahashi M, Bamburg JR (1998). Actin depolymerizing factor and cofilin phosphorylation dynamics: response to signals that regulate neurite extension. Cell Motil Cytoskeleton 39, 172–190.

Meyn MA 3rd, Smithgall TE (2008). Small molecule inhibitors of Lck: the search for specificity within a kinase family. Mini Rev Med Chem 8, 628–637.

Mishima T, Naotsuka M, Horita Y, Sato M, Ohashi K, Mizuno K (2010). LIM-kinase is critical for the mesenchymal-to-amoeboid cell morphological transition in 3D matrices. Biochem Biophys Res Commun 392, 577–581.

Mizuno K (2013). Signaling mechanisms and functional roles of cofilin phosphorylation and dephosphorylation. Cell Signal 25, 457–469.

Mizuno K, Okano I, Ohashi K, Nunoue K, Kuma K, Miyata T, Nakamura T (1994). Identification of a human cDNA encoding a novel protein kinase with two repeats of the LIM/double zinc finger motif. Oncogene 9, 1605–1612.

Nagai T, Ibata K, Park ES, Kubota M, Mikoshiba K, Miyawaki A (2002). A variant of yellow fluorescent protein with fast and efficient maturation for cell-biological applications. Nat Biotechnol 20, 87–90.

Nishita M, Aizawa H, Mizuno K (2002). Stromal cell-derived factor 1alpha activates LIM kinase 1 and induces cofilin phosphorylation for T-cell chemotaxis. Mol Cell Biol 22, 774–783.

Nishita M, Tomizawa C, Yamamoto M, Horita Y, Ohashi K, Mizuno K (2005). Spatial and temporal regulation of cofilin activity by LIM kinase and Slingshot is critical for directional cell migration. J Cell Biol 171, 349–359.

Ohashi K, Fujiwara S, Watanabe T, Kondo H, Kiuchi T, Sato M, Mizuno K (2011). LIM kinase has a dual role in regulating lamellipodium extension by decelerating the rate of actin retrograde flow and the rate of actin polymerization. J Biol Chem 286, 36340–36351.

Ohashi K, Kiuchi T, Shoji K, Sampei K, Mizuno K (2012). Visualization of cofilin-actin and Ras-Raf interactions by bimolecular fluorescence complementation assays using a new pair of split Venus fragments. Biotechniques 52, 45–50.

Ohashi K, Nagata K, Maekawa M, Ishizaki T, Narumiya S, Mizuno K (2000). Rho-associated kinase ROCK activates LIM-kinase 1 by phosphorylation at threonine 508 within the activation loop. J Biol Chem 275, 3577–3582.

Oikawa M (2010). An improved synthesis of arylboronates toward twenty novel 1,3-disubstituted 4-amino-1h-pyrazolo[3,4-D]pyrimidine analogs. Heterocycles 81, 73–77.

Oikawa M, Ikoma M, Sasaki M (2005). Simultaneous accumulation of both skeletal and appendage-based diversities on tandem Ugi/Diels-Alder products. Tetrahedron Lett 46, 5863–5866.

Oikawa M, Ueno T, Oikawa H, Ichihara A (1995). Total synthesis of tautomycin. J Org Chem 60, 5048–5068.

Okano I, Hiraoka J, Otera H, Nunoue K, Ohashi K, Iwashita S, Hirai M, Mizuno K (1995). Identification and characterization of a novel family of serine/threonine kinases containing two N-terminal LIM motifs. J Biol Chem 270, 31321–31330.

Ono S (2007). Mechanism of depolymerization and severing of actin filaments and its significance in cytoskeletal dynamics. Int Rev Cytol 258, 1–82.

Parker C *et al.* (2010). Effect of mitoxantrone on outcome of children with first relapse of acute lymphoblastic leukaemia (ALL R3): an open-label randomised trial. Lancet 376, 2009–2017.

Pollard TD, Borisy GG (2003). Cellular motility driven by assembly and disassembly of actin filaments. Cell 112, 453–465.

Prudent R *et al.* (2012). Pharmacological inhibition of LIM kinase stabilizes microtubules and inhibits neoplastic growth. Cancer Res 72, 4429–4439.

Ross-Macdonald P *et al.* (2008). Identification of a nonkinase target mediating cytotoxicity of novel kinase inhibitors. Mol Cancer Ther 7, 3490–3498.

Saito A, Miyajima K, Akatsuka J, Kondo H, Mashiko T, Kiuchi T, Ohashi K, Mizuno K (2013). CaMKII beta-mediated LIM-kinase activation plays a crucial role in BDNF-induced neuritogenesis. Genes Cells 18, 533–543.

Schlessinger J, Lemmon MA (2003). SH2 and PTB domains in tyrosine kinase signaling. Sci STKE 2003, RE12.

Scott RW *et al.* (2010). LIM kinases are required for invasive path generation by tumor and tumor-associated stromal cells. J Cell Biol 191, 169–185.

Scott RW, Olson MF (2007). LIM kinases: function, regulation and association with human disease. J Mol Med (Berl) 85, 555–568.

Shoji K, Ohashi K, Sampei K, Oikawa M, Mizuno K (2012). Cytochalasin D acts as an inhibitor of the actin-cofilin interaction. Biochem Biophys Res Commun 424, 52–57.

Sleebs BE, Nikolakopoulos G, Street IP, Falk H, Baell JB (2011). Identification of 5,6-substituted 4-aminothieno[2,3-*d*]pyrimidines as LIMK1 inhibitors. Bioorg Med Chem Lett 21, 5992–5994.

Toshima J, Toshima JY, Amano T, Yang N, Narumiya S, Mizuno K (2001). Cofilin phosphorylation by protein kinase testicular protein kinase 1 and its role in integrin-mediated actin reorganization and focal adhesion formation. Mol Biol Cell 12, 1131–1145.

Tzivion G, Avruch J (2002). 14-3-3 proteins: active cofactors in cellular regulation by serine/threonine phosphorylation. J Biol Chem 277, 3061–3064.

Wang W, Eddy R, Condeelis J (2007). The cofilin pathway in breast cancer invasion and metastasis. Nat Rev Cancer 7, 429–440.

Yang N, Higuchi O, Ohashi K, Nagata K, Wada A, Kangawa K, Nishida E, Mizuno K (1998). Cofilin phosphorylation by LIM-kinase 1 and its role in Rac-mediated actin reorganization. Nature 393, 809–812.

Yoshioka K, Foletta V, Bernard O, Itoh K (2003). A role for LIM kinase in cancer invasion. Proc Natl Acad Sci USA 100, 7247–7252.

Nonmetal Haptens Induce ATP Release from Keratinocytes through Opening of Pannexin Hemichannels by Reactive Oxygen Species

Kaoru Onami[1], Yutaka Kimura[1], Yumiko Ito[1], Takeshi Yamauchi[1], Kenshi Yamasaki[1] and Setsuya Aiba[1]

Although extracellular adenosine 5′-triphosphate (eATP) has a crucial role in the sensitization phase of contact hypersensitivity (CHS), the mechanism by which hapten causes keratinocyte cell death and ATP release is unknown. We examined the time course of cell death, reactive oxygen species (ROS) production, and ATP release in HaCaT cells and in normal human keratinocytes after exposure to nonmetal haptens, $NiCl_2$, or irritants. Both haptens and irritants caused cell death of keratinocytes but with different time courses. *N*-acetylcysteine (NAC) significantly reduced only nonmetal hapten-induced cell death as assessed by propidium iodide exclusion. We examined the effects of antioxidants and pannexin (Panx) inhibitors on cell death, ROS production, and ATP release by chemical-treated HaCaT cells. Nonmetal hapten-induced cell death, but not $NiCl_2$- or irritant-related cell death, was dependent on reactivity to thiol residues in the cells. NAC reduced cell death and ATP release, whereas antioxidants and Panx inhibitors did not inhibit cell death but significantly attenuated ATP release. Panx1 small interfering RNA (siRNA) also suppressed ATP release from hapten-exposed HaCaT cells. Intraperitoneal injection of a Panx1 inhibitor attenuated murine CHS. These findings suggest that nonmetal hapten reactivity to thiol residues causes membrane disruption of keratinocytes and ROS production that leads to ATP release through opening of Panx hemichannels.

Journal of Investigative Dermatology (2014) **134,** 1951–1960; doi:10.1038/jid.2014.93; published online 17 April 2014

INTRODUCTION

Sensitization to contact allergens requires activation of the innate immune system that leads to dendritic cell (DC) activation. However, the mechanisms by which contact allergens activate innate immune signaling pathways are incompletely understood. It is possible that "endogenous danger signals" or "damage-associated molecular patterns" (reviewed in Willart and Lambrecht, 2009) are responsible for activation of the innate immune system in allergic sensitization. The following molecules have been identified as damage-associated molecular patterns: adenosine 5′-triphosphate (ATP), heat shock proteins, hyaluronic acid, monosodium urate, galectins, thioredoxin, adenosine, high-mobility group box protein 1, IL-1α, and IL-33 (reviewed in Hirsinger *et al.*, 2012).

Recent studies using gene targeting in mice demonstrated that Toll-like receptor 2 (TLR2)/TLR4 double-deficient mice (Martin *et al.*, 2008) or purinergic receptor $P2X_7$-deficient mice (Weber *et al.*, 2010) are resistant to allergic contact hypersensitivity (CHS), indicating an essential role of TLR2/TLR4 as well as of purinergic receptor $P2X_7$ in the mouse CHS model. Breakdown products of hyaluronic acid in the range of 1.2 to 500 kDa that are generated during inflammation or tissue damage have been demonstrated to stimulate TLR2 and/or TLR4 in immune cells such as macrophages or DCs (Termeer *et al.*, 2002; Scheibner *et al.*, 2006). Indeed, Esser *et al.* (2012) reported that haptens induce reactive oxygen species (ROS) production by keratinocytes *in vitro* as well as *in vivo*, thereby increasing hyaluronidase activity in the skin that results in the production of low-molecular-weight hyaluronic acid fragments. Combined, these observations suggest that hapten-exposed keratinocytes generate pro-inflammatory low-molecular-weight hyaluronic acid fragments that induce CHS via stimulation of TLR2/TLR4.

Similarly, extracellular ATP (eATP) released by stressed or damaged cells can also activate innate immune responses. The transmembrane ATP receptor $P2X_7$ has been implicated in the post-translational processing of pro-IL-1β and pro-IL-18 via activation of the NLRP3 inflammasome (reviewed by Vitiello *et al.*, 2012). Although Weber *et al.* (2010)

[1]*Department of Dermatology, Tohoku University Graduate School of Medicine, Sendai, Japan*

Correspondence: Setsuya Aiba, Department of Dermatology, Tohoku University Graduate School of Medicine, 1-1 Seiryo-machi, Aoba-ku, Sendai, 980-8574, Japan. E-mail: saiba@med.tohoku.ac.jp

Abbreviations: ATP, adenosine 5′-triphosphate; CBX, carbenoxolone; CHS, contact hypersensitivity; DC, dendritic cell; DNCB, dinitrochlorobenzene; DPCP, diphenylcyclopropenone; eATP, extracellular ATP; LA, lactic acid; LDH, lactate dehydrogenase; NAC, N-acetylcysteine; 4-NBB, 4-nitrobenzylbromide; NHEK, normal human epidermal keratinocyte; Panx, pannexin; PI, propidium iodide; ROS, reactive oxygen species; siRNA, small interfering RNA; TLR, Toll-like receptor

Received 26 September 2013; revised 30 January 2014; accepted 3 February 2014; accepted article preview online 14 February 2014; published online 17 April 2014

demonstrated eATP release in skin painted with hapten, they did not address the mechanism by which hapten-treated keratinocytes release ATP.

In this study, we compared the effects of haptens with irritants on keratinocyte cell death, ROS generation, and ATP release. Although the generation of ROS by hapten-exposed keratinocytes has been demonstrated in several studies (Mehrotra *et al.*, 2005; Esser *et al.*, 2012; Kim *et al.*, 2012), the effect of the generated ROS on cell death and ATP release from hapten-exposed keratinocytes has not been examined. First, we demonstrated that haptens and irritants caused the cell death of the human keratinocyte cell line HaCaT and normal human epidermal keratinocytes (NHEKs), and induced ATP release with different time courses. *N*-acetylcysteine (NAC) significantly reduced cell death of HaCaT cells exposed to haptens but did not affect the death of cells exposed to irritants. Three representative nonmetal haptens, dinitrochlorobenzene (DNCB), 4-nitrobenzylbromide (4-NBB), and diphenylcyclopropenone (DPCP), induced the generation of ROS in HaCaT cells that was significantly attenuated by pretreatment with NAC and several antioxidants. Despite the inhibitory effects of NAC and antioxidants on ROS generation, antioxidants suppressed lactate dehydrogenase (LDH) activity and ATP release but did not affect cell death that was assessed using propidium iodide (PI) exclusion. In addition, studies using pannexin (Panx) inhibitors revealed that ATP release from hapten-treated HaCaT cells was through Panx hemichannels. Furthermore, intraperitoneal injection of a pannexin inhibitor, carbenoxolone (CBX), significantly attenuated CHS induced by DNCB. Combined, these results provide an insight into the mechanism by which haptens cause keratinocyte death and ATP release in CHS.

RESULTS

Both haptens and irritants induce HaCaT and NHEK cell death and ATP release but with different time courses

Evaluation of cell death by PI exclusion using flow cytometry and LDH release assay showed that two nonmetal haptens DNCB and 4-NBB, one metal hapten $NiCl_2$, and two irritants SDS and lactic acid (LA) induced HaCaT cell death in a dose-dependent manner (Figure 1a). The minimum concentrations of reagents that were toxic to all cells were 100 μM for DNCB and 4-NBB, 6 mM for $NiCl_2$, 250 μM for SDS, and 34 mM for LA. Haptens and irritants induced cell death with different time courses: maximum cell death was evident 1 hour after irritant exposure but maximum cell death was only achieved after more than 6 hours of hapten exposure as assessed by PI staining. LDH activity in culture supernatants was increased 6 hours after hapten exposure, whereas maximum release of LDH was seen 1 hour after SDS exposure. The LDH activity of LA-treated HaCaT cells could not be measured, possibly because of disturbance of LDH enzyme activity due to the acidity of culture supernatants containing LA.

The time course of ATP release was also different between haptens and irritants. ATP release was evident 6 hours after hapten exposure, whereas maximum ATP release was seen 1 hour after exposure to irritants (Figure 1a). To test whether higher concentrations of hapten induce an earlier release of ATP, HaCaT cells were incubated with increased concentrations of DNCB (from 100 μM to 3.2 mM); however, ATP release earlier than 6 hours after DNCB exposure was not observed (data not shown). To clarify whether the delayed ATP release is limited to HaCaT cells, ATP release in culture supernatants of NHEKs exposed to either haptens or irritants was assessed. Similar to HaCaT cells, the time course of ATP release from NHEKs was also different between haptens and irritants (Figure 1b).

NAC attenuates HaCaT cell death caused by DNCB, 4-NBB, and DPCP but does not affect cell death caused by $NiCl_2$, SDS, or LA

We previously reported that haptens induce a redox imbalance in DCs that stimulates the phosphorylation of p38 mitogen-activated protein kinase and DC activation, and that pretreatment of DCs with NAC corrects the redox imbalance and abrogates the phosphorylation of p38 mitogen-activated protein kinase as well as DC activation (Mizuashi *et al.*, 2005). Therefore, we examined whether NAC could attenuate cell death caused by haptens and irritants. NAC significantly suppressed HaCaT cell death caused by nonmetal haptens DNCB, 4-NBB, and DPCP, as assessed by PI-positive cells, but did not affect cell death caused by a metal hapten $NiCl_2$, or irritants SDS or LA (Figure 2). Similarly, ATP release and LDH activity of HaCaT cells 12 hours after DNCB, 4-NBB, or DPCP exposure were significantly attenuated by NAC, but NAC had little effect on ATP release and LDH activity induced by $NiCl_2$, LA, or SDS (Figure 2).

HaCaT cells exposed to haptens and irritants produce ROS and mitochondrial superoxide anion depending on their thiol reactivity

Next, we examined whether exposure of HaCaT cells to haptens or irritants results in production of ROS using the CM-H_2DCFDA probe (Figure 3a). All nonmetal haptens but not the metal hapten $NiCl_2$ stimulated intracellular ROS production in a dose-dependent manner from 30 minutes to 6 hours after stimulation. ROS production in HaCaT cells exposed to DNCB or DPCP was greater than that in cells exposed to 4-NBB. SDS exposure resulted in the production of ROS in HaCaT cells from 30 minutes to 24 hours after exposure, but the amount of ROS production in the first 6 hours after exposure was much smaller than that caused by hapten exposure. The concentration of SDS that induced cell death of the majority of HaCaT cells did not result in a significant amount of ROS generation within 1 hour after exposure, suggesting that ROS did not contribute to SDS-related HaCaT cell death. LA did not induce ROS in keratinocytes. The positive control H_2O_2 triggered immediate production of ROS in HaCaT cells.

As pretreatment with NAC significantly attenuated HaCaT cell death as well as ATP release, we examined the effects of NAC on ROS production by hapten-exposed HaCaT cells. Pretreatment of HaCaT cells with NAC significantly attenuated ROS production by hapten-exposed HaCaT cells 6 hours after exposure, whereas it did not significantly affect ROS production by SDS- or H_2O_2-treated HaCaT cells (Figure 3b).

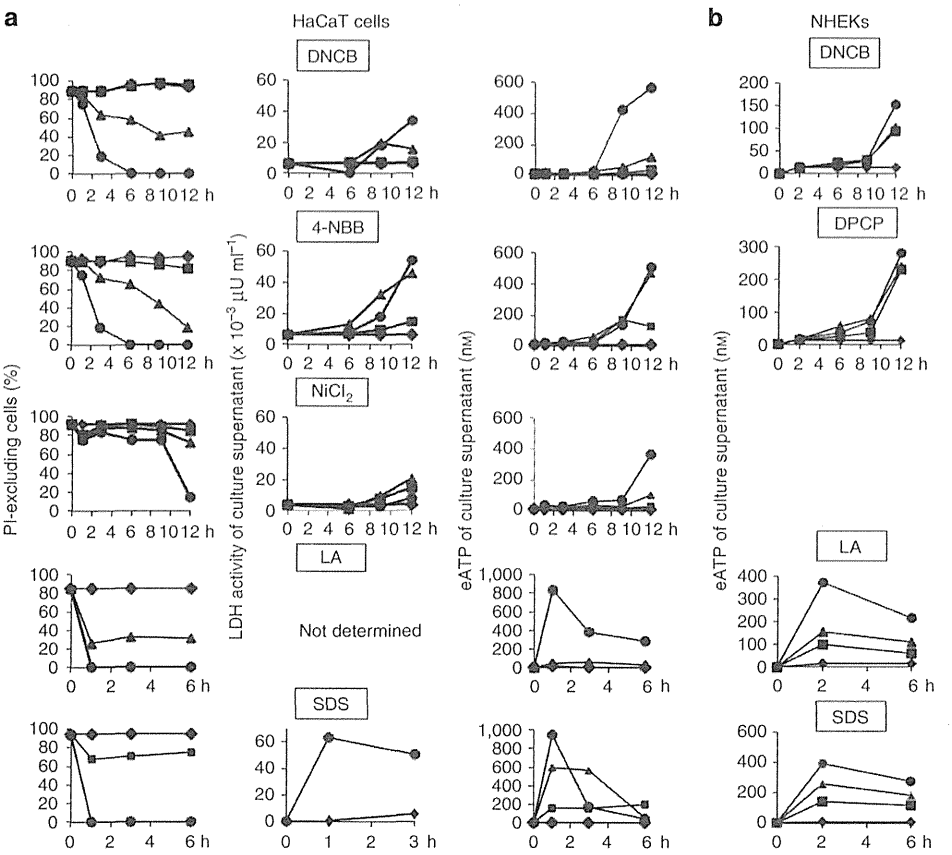

Figure 1. Haptens and irritants cause cell death of HaCaT cells and induce adenosine 5′-triphosphate (ATP) release with different time courses. (**a**) HaCaT cells or (**b**) normal human epidermal keratinocytes (NHEKs) cultured in 24-well plates were treated with graded concentrations of haptens dinitrochlorobenzene (DNCB), 4-nitrobenzylbromide (4-NBB), diphenylcyclopropenone (DPCP), or $NiCl_2$, or irritants lactic acid (LA) or SDS, for various time periods. After incubation, propidium iodide (PI) exclusion, lactate dehydrogenase (LDH) activity, and ATP release were examined to assess cell viability. The mean LDH activity and extracellular ATP (eATP) release of triplicate cultures were calculated for each chemical. The symbols ●, ▲, ■, and ◆ correspond to the highest, medium, and lowest concentrations and vehicle control of each chemical, respectively. Chemicals and their concentrations were as follows: DNCB, 4-NBB, and DPCP—100, 50, and 25 μM; $NiCl_2$—6.0, 3.0, and 1.5 mM; SDS—250, 125, and 62.5 μM; and LA—34 and 17 mM. Representative data from three independent experiments are shown.

Next, to clarify the source of ROS in HaCaT cells treated with haptens, we examined whether haptens induce mitochondrial superoxide anion generation using MitoSOX, a mitochondria-targeted ROS-specific fluorescent probe. DNCB, DPCP, and 4-NBB, although weakly, induced mitochondrial superoxide anion production 2 hours after cell exposure (Figure 3c), suggesting that mitochondria contribute to ROS production in HaCaT cells exposed to nonmetal haptens. Treatment with H_2O_2 also induced mitochondrial superoxide anion production. Pretreatment with NAC significantly attenuated mitochondrial superoxide anion production in HaCaT cells exposed to DNCB, 4-NBB, or DPCP, although its inhibitory effect on superoxide anion production by HaCaT cells exposed to 4-NBB was minimum (Figure 3c).

TEMPOL and apocynin do not rescue hapten-treated HaCaT cells from cell death but suppress ROS production and reduce ATP release

Although ROS production after hapten stimulation in the mitochondria of dendritic cells (Migdal *et al.*, 2010) and in the cytosol of keratinocytes (Mehrotra *et al.*, 2005) has been documented, the source of ROS production that causes keratinocyte cell death and ATP release has not yet been determined. Therefore, we examined whether the following reagents affect ROS production in hapten-exposed HaCaT cells: TEMPOL, a whole-cell antioxidant (Wilcox and Pearlman, 2008); MnTBAP, a superoxide dismutase mimetic, catalase mimetic, and peroxynitrite scavenger (Konorev *et al.*, 2002; Batinic-Haberle *et al.*, 2009); allopurinol, a xanthine oxidase inhibitor (Borges *et al.*, 2002); and apocynin, an NADPH oxidase inhibitor (Bedard and Krause, 2007). Results showed that TEMPOL, MnTBAP, and apocynin suppressed ROS production by HaCaT cells exposed to DNCB, 4-NBB, and DPCP, but their inhibitory effect on ROS production by 4-NBB-treated HaCaT cells was not statistically significant (Figure 4a). In contrast, allopurinol failed to suppress ROS production in HaCaT cells exposed to haptens.

We also examined whether MnTBAP or TEMPOL suppresses mitochondrial superoxide anion production by